# THE SEEBECK EFFECT IN THIN FILM CdS AND $Zn_xCd_{1-x}S$

by

Scott Preston Moore

Thesis submitted to the Graduate Faculty of the

Virginia Polytechnic Institute and State University

in partial fulfillment of the requirements for the degree of

MASTER OF SCIENCE

in

Materials Engineering

APPROVED:

L. C. Burton, Chairman

J. J. Brown, Jr.

J. L. Lytton

May, 1982

Blacksburg, Virginia

Acknowledgements

The author wishes to extend thanks, first, to Dr. L. C. Burton for his guidance and patience as the author's graduate advisor and chairman of the graduate committee. Second, to Dr. J. J. Brown and Dr. J. L. Lytton for serving on the author's graduate committee. Also to Dr. M. K. Rao, P. Uppal, and H. Naseem for their assistance and suggestions. Finally the author wishes to thank Pam Tipsword and Teresa Engle for proofreading and Karen Kessinger for typing the manuscript.

TABLE OF CONTENTS

LIST OF TABLES

LIST OF FIGURES

# I. Introduction

## 1.1 The Seebeck Effect in Thin Film Samples

The development of any device depends not only on the physical theory behind its operation, but also on experimental techniques which help to improve its operation to a more efficient and thus economical level. The ability to produce high quality, semiconducting thin films is essential in the development of high efficiency thin film photovoltaic solar cells. Materials properties such as composition, grain size, and dislocation density strongly affect a film's electrical characteristics. These properties must be controlled to produce electrical characteristics in each film which benefit the conversion ability of the cell.

Electrical characteristics such as mobility, carrier concentration, and the position of the Fermi level have been traditionally measured by Hall effect and resistivity measurements. Another method for determining these characteristics is by measuring the Seebeck or thermoelectric voltage. This is a somewhat easier measurement at a given temperature because the magnetic field needed for Hall measurements is not required. In addition the measured Hall voltage is proportional to the carrier mobility, whereas the measured Seebeck voltage is directly related to carrier density. The Seebeck measurements are thus more useful in the characterization of low-mobility materials where Hall measurements may be difficult.

When a temperature gradient ($\Delta T$) exists across a sample under open-circuit conditions a voltage ($\Delta V$) is generated by the sample. This is the Seebeck or thermoelectric voltage. In a semiconducting material

the polarity of the voltage will depend on the type of material (n or p). If the sample is n-type as shown in Figure 1, the cold end of the sample takes the sign of the majority carrier (negative). For the p-type sample, the cold end becomes positive. The polarity of the Seebeck voltage is useful in early materials characterization in determining the sign of the majority carrier.

The Seebeck voltage generated by the sample is due to two effects: (1) the spreading out of the Fermi distribution with increasing temperature and, (2) the change in the Fermi energy with temperature. There is an overall increase in the population of higher energy majority carriers at the hot end of the sample. Diffusion of these carriers towards the cold end of the sample results in the development of a potential in the opposite direction. The voltage that is developed is proportional to the temperature gradient. The Seebeck coefficient is defined as follows:[1]

$$\alpha = \frac{\Delta V}{\Delta T} \qquad 1.1$$

where $\Delta V$ and $\Delta T$ were defined previously. The Seebeck coefficient ranges from $10^{-4}$ to $10^{-3}$ volts/deg. for extrinsic semiconductors.

The Seebeck coefficient is related to the position of the Fermi level and to an energy transport term, S. This relation has the form for electrons:[2]

$$\alpha_e = -\frac{K}{e}\left[\left(\frac{5}{2} - S\right) + \frac{E_c - E_F}{KT}\right] \qquad 1.2$$

where $E_F$ is the Fermi energy, $E_c$ is the conduction band energy, e is electronic charge and K is the Boltzmann constant. The difference

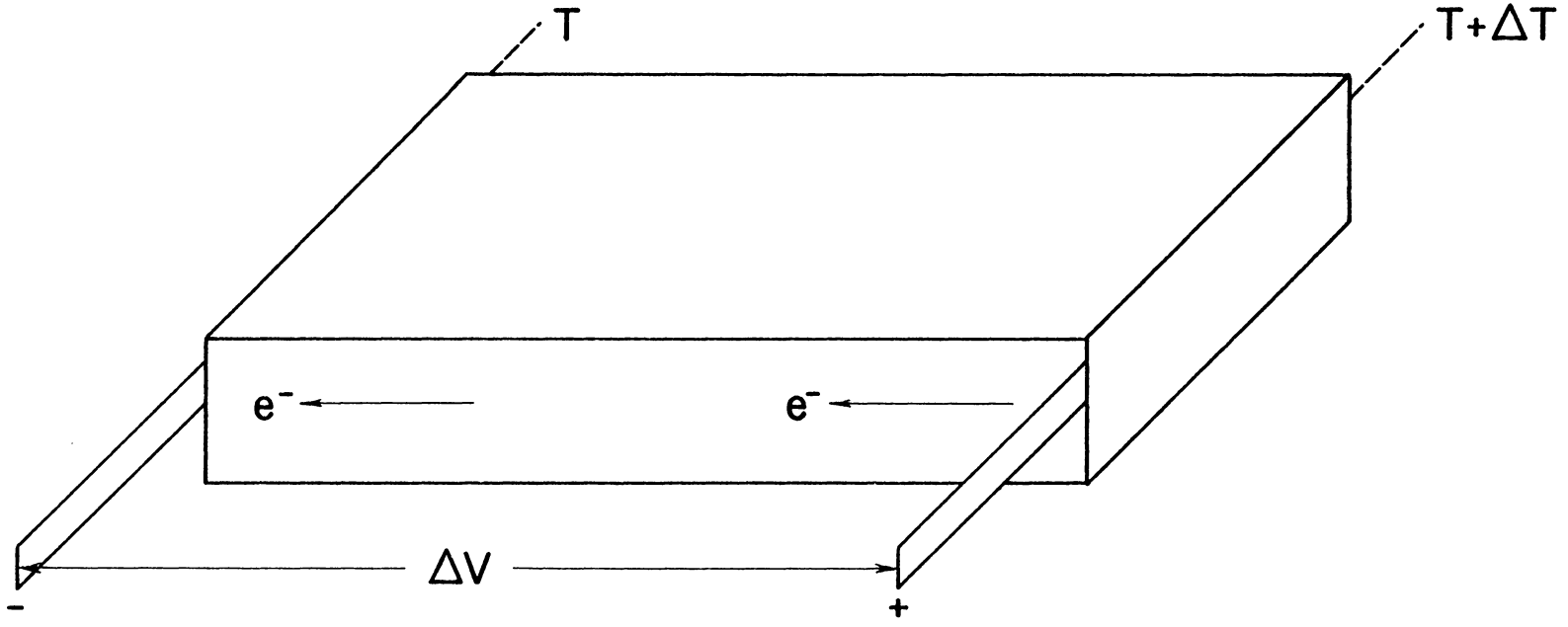


Figure 1. When a temperature gradient ΔT is applied to an n-type sample electrons flow from the high temperature end. A potential ΔV is developed to allow for the transfer of energy.

between the conduction band energy and the Fermi energy leads directly to the carrier concentration (discussed in greater detail later). The drift mobility for the majority carrier can then be calculated at a given temperature from the relation:

$$\mu = \frac{1}{ne\rho} \qquad 1.3$$

once the carrier concentration n and resistivity $\rho$ have been found (e being the electronic charge). A derivation of equation 1.2 from Boltzmann's transport equation is found in Chapter 2.

The change in mobility with respect to temperature gives an indication of the predominant form of scattering of majority carriers. Scattering is largely due to impurities, phonons, grain boundaries, and defects.

In a polycrystalline film the two predominant scattering modes are due to phonons and grain boundaries. Electrostatic potential barriers are associated with grain boundaries. The Petritz theory in polycrystalline semiconductor films predicts:[3]

$$\mu = \mu_o \exp(-\phi_b/KT) \qquad 1.4$$

where $\phi_b$ is the intergrain barrier height, and $\mu_o$ is related to the grain size and has been found by J. W. Orton et al.[4] to vary strongly with $\phi_b$. This can only be understood if $\phi_b$ is temperature dependent. If scattering is dominated by a mechanism within the grain such as phonon or impurity scattering, mobility is usually proportional to $T^n$. In the case of acoustic phonon scattering the mobility is proportional to $T^{-3/2}$.[5] Impurity scattering usually predominates at low temperatures ($\lesssim$ 100 K) and mobility follows a $T^{3/2}$ dependence.[6]

## 1.2 CdS and ZnCdS Studies

The essential component of a photovoltaic solar cell is a p-n junction. According to the conventional heterojunction model, when photons with energy greater than the energy gap traverse the vicinity of the junction, electron-hole pairs are created in the materials on both sides of the junction. In the "backwall" mode of operation, one of the semiconductors serves as a solar window. That is, ideally it would have a large enough band gap to not absorb any of the incident photons. This ideality is approached by CdS which has a large band gap (2.4 eV) and is n-type due to naturally occurring defects. The other (p-type) semiconductor serves as an absorber. That is, ideally an electron-hole pair would be created by each incident photon. In reality considerable loss of energy occurs for photons having energies higher than the energy gap of the absorber material. This energy is lost to the lattice as heat as the excited carriers are scattered from energies above the band edge into states near the band edge. Energy is also lost when the photons have energy less than the energy gap of the absorber material, since these photons are not absorbed.

The most efficient all-thin-film solar cell to date is the $CdS/Cu_2S$ type shown in Figure 2. This cell can be illuminated in either a "frontwall" or "backwall" configuration. The CdS window material must have low resistance to minimize series resistance losses, and therefore high mobility. A $Cu_2S/Zn_xCd_{1-x}S$ cell (using the ternary $Zn_xCd_{1-x}S$ in place of the CdS) is also of interest because it offers potentially 50% more voltage than is available from the $Cu_2S/CdS$ cell.[8]

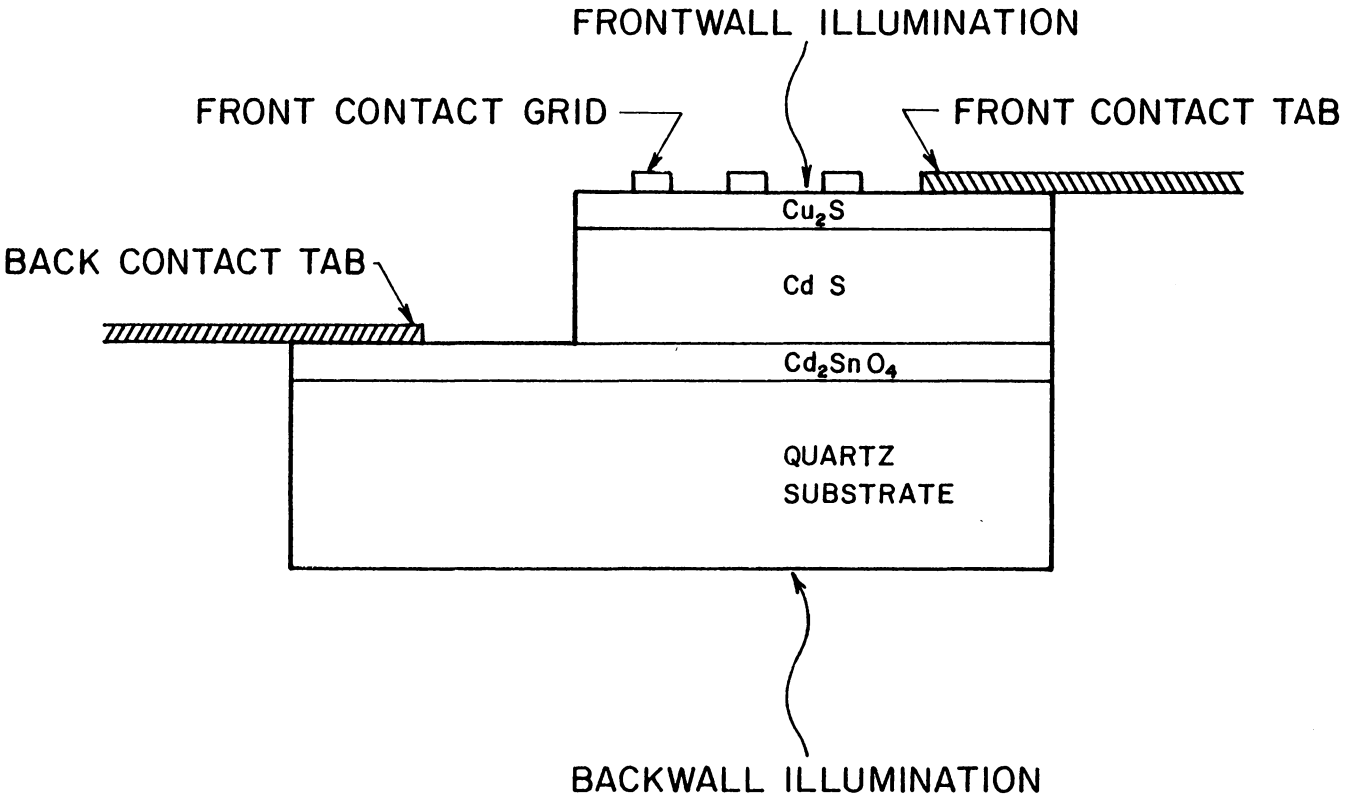


Figure 2. Schematic of $CdS/Cu_2S$ solar cell indicating backwall and frontwall illumination.[7]

The advantage of $Zn_xCd_{1-x}S$ over CdS is the decrease in the lattice constant which provides for a closer lattice match with the $Cu_2S$ film. Crystallographic defects at the junction, which are sites for electron-hole recombination, are thus reduced. Also the electron affinity of $Zn_xCd_{1-x}S$ better matches that of $Cu_2S$, providing for increased cell voltage.

Seebeck measurements can be used to characterize the quality of thin film solar cell materials, such as CdS and ZnCdS. The Seebeck effect has been used to measure the transport properties in CdS single crystals by Kwok and Bube.[9] Mobility was found to be dominated by optical mode lattice scattering at higher temperatures (> 200 K) and by charged impurity scattering at lower temperatures (< 200 K). A phonon drag contribution was observed which decreased with increasing degeneracy. The Seebeck effect was used in the characterization of solution-sprayed and evaporated CdS films by Wu and Bube.[10] Sprayed films had thicknesses between 0.70 and 1.80 μm. Electron concentrations in the range of $4X10^{16}$ to $1.5X10^{17}$ $cm^{-3}$ were reported. Electron mobilities were reported to be thermally activated and dependent on grain boundary scattering. Grain boundary barrier heights ($\phi$) were reported as 0.11, 0.13, and 0.22 eV on three sprayed samples, and $\mu_o$ as 100,3, and 5 $cm^2$/volt.sec., respectively. Evaporated films had thicknesses of about 2.2 μm. Electron densities ranged from $6X10^{15}$ to $3.5X10^{19}cm^{-3}$. Mobilities varied from 0.13 to 6.3 $cm^2$/volt. sec. at 300K. Electrical transport properties were examined for sprayed $Zn_xCd_{1-x}S$ films by Chynoweth and Bube.[11] They reported that as the

proportion of Zn increased the carrier concentration n decreased according to the relation

$$\ell n\ n = 38.40 - 29x$$

where x is the atomic fraction of Zn in the film. The resistivity increased from 12.8 Ω-cm with no zinc added to $5.0X10^6$ Ω-cm at a Zn content of 35 atomic percent. The mobility decreased with increasing Zn content (0 to 35 atomic percent) from 10.5 to 0.6 $cm^2$/volt. sec. The films varied in thickness from 0.83 to 2.55 μm. There was no attempt made to correlate the change in mobility and resistivity with film thickness.

## 1.3 Objectives of This Work

As noted above, the Seebeck effect has been used to study the transport properties in sprayed and evaporated CdS films. However, no work has been reported on evaporated $Zn_xCd_{1-x}S$ films or on the effect of thickness on the thermoelectric properties of evaporated CdS films. Thus, the objectives of this study were:

1. To design and build an apparatus to measure the Seebeck effect and resistivity in thin film CdS and $Zn_xCd_{1-x}S$ films over a wide temperature range.
2. To find mobility and carrier concentration values from Seebeck effect and resistivity measurements as functions of temperature on evaporated CdS samples of varying thicknesses, and on evaporated $Zn_xCd_{1-x}S$ samples of varying zinc content (using Hall measurements in some cases as a check for mobility values at room temperature).
3. To determine the dominant scattering mechanisms from the temperature dependence of mobility.

Theory related to the Seebeck effect is discussed in the next chapter. The following chapters deal with experimental techniques, results, and conclusions.

# II. Theory

## 2.1. General

The distribution of electrons in a crystal can be expressed as $f(\vec{k}, \vec{r}, t)$ where t is time, $\vec{k}$ is the wave vector of the electron, and $\vec{r}$ is the position vector of the electron. The rate of change of this distribution function, which describes the occupancy of allowed energy states involved in transport processes, is given by:

$$\frac{df}{dt} = \frac{\partial f}{\partial t}\Big]_{\text{external field}} + \frac{\partial f}{\partial t}\Big]_{\text{diffusion}} + \frac{\partial f}{\partial t}\Big]_{\text{scattering}} \qquad 2.1$$

The change in the distribution function due to an applied external field is given by:

$$\frac{\partial f}{\partial t}\Big]_{\text{external field}} = -\frac{\partial \vec{k}}{\partial t} \cdot \nabla_{\vec{k}} f \qquad 2.2$$

where $\frac{\partial \vec{k}}{\partial t}$ is the first derivative of the wave vector with respect to time and $\nabla_{\vec{k}} f$ is the gradient operator, acting on f, which is taken with respect to the components of the wave vector $\vec{k}$. Using the following:

$$\dot{\vec{k}} = \frac{d\vec{k}}{dt} = \frac{\vec{F}}{\hbar} \qquad 2.3$$

where $\hbar$ is Planck's constant divided by $2\pi$ and F is the external force, equation 2.2 can be rewritten:

$$\frac{\partial f}{\partial t}\Big]_{\text{external field}} = -\frac{\vec{F}}{\hbar} \cdot \nabla_{\vec{k}} f \qquad 2.4$$

The change in the distribution function due to diffusion is given by:

$$\left.\frac{\partial f}{\partial t}\right|_{\text{diffusion}} = -\frac{d\vec{r}}{dt} \cdot \nabla_{\vec{r}} f \qquad 2.5$$

where $\frac{d\vec{r}}{dt}$ is the first derivative of the position vector with respect to time and $\nabla_{\vec{r}} f$ is the gradient operator, acting on f, with respect to spatial coordinates. Equation 2.5 can be rewritten:

$$\left.\frac{\partial f}{\partial t}\right|_{\text{diffusion}} = -\vec{V} \cdot \nabla_{\vec{r}} f \qquad 2.6$$

where $\vec{V}$ is the velocity vector of the electrons. Under steady-state conditions $\frac{df}{dt} = 0$, and equation 2.1 can be rewritten:

$$\left.\frac{df}{dt}\right|_{\text{scattering}} = \frac{\vec{F}}{\hbar} \cdot \nabla_{\vec{k}} f + \vec{V} \cdot \nabla_{\vec{r}} f \qquad 2.7$$

If the probability per unit time for scattering electrons from a state $\vec{k}$ to a state $\vec{k}'$ is $P_{\vec{k}\vec{k}'}$, then the scattering component can be written:

$$\left.\frac{\partial f}{\partial t}\right|_{\text{scattering}} = \{P_{\vec{k}'\vec{k}} f(\vec{k}')[1-f(\vec{k})] - P_{\vec{k}\vec{k}'} f(\vec{k})[1-f(\vec{k}')]\}d\vec{k}' \qquad 2.8$$

At equilibrium the energy distribution of the electron is given by the Fermi-Dirac distribution:

$$f(\vec{k}, \vec{r}, t) = f_o(E) = \frac{1}{\exp[(E-E_F)/KT]+1} \qquad 2.9$$

where $E_F$ is the Fermi level and K is the Boltzmann constant. Also at equilibrium there is no change in the density function due to scattering $(\partial f/\partial t]_{\text{scattering}} = 0)$ therefore:

$$P_{\vec{k}\vec{k}} = P_{\vec{k}\vec{k}'} \frac{f_o(E)[1 - f_o(E')]}{f_o(E')[1 - f_o(E)]} \qquad 2.10$$

If the system moves away from equilibrium, the distribution function is changed by an amount $f'(\vec{k},\vec{r})$: i.e.

$$f(\vec{k}, \vec{r}) = f_o(E) + f'(\vec{k}, \vec{r}) \qquad 2.11$$

The departure from equilibrium can be written:

$$f'(\vec{k}, \vec{r}) = -\phi(\vec{k}, \vec{r}) \frac{\partial f_o}{\partial E} \qquad 2.12$$

If equations 2.10 through 2.12 are substituted into equation 2.8, it becomes:

$$\left.\frac{\partial f}{\partial t}\right]_{} = \frac{1}{KT} \int P_{\vec{k}\vec{k}'} f_o(E)[1 - f_o(E')][\phi(\vec{k}') - \phi(k)]d\vec{k}' \qquad 2.13$$

If the external force is caused by an electric field $(\vec{\varepsilon})$ then $\vec{F} = e\vec{\varepsilon}$ and equation 2.7 can be written:

$$\left.\frac{\partial f}{\partial t}\right]_{\text{scattering}} = \frac{e\vec{\varepsilon}}{} \cdot \nabla_{\vec{k}} f + \frac{1}{h} \nabla_{\vec{k}} E(\vec{k}) \cdot \nabla_{\vec{r}} f \qquad 2.14$$

where $\vec{V}$ in equation 2.6 has been replaced by $\frac{1}{h} \nabla_{\vec{k}} E(\vec{k})$. If scattering is described in terms of a relaxation time $\tau$ then:

$$\left.\frac{\partial f}{\partial t}\right]_{\text{scattering}} = \frac{e\vec{\varepsilon}}{} \cdot \nabla_{\vec{k}} f + \frac{1}{} \nabla_{\vec{k}} E(\vec{k}) \cdot \nabla_{\vec{r}} f = -\frac{f'}{\tau} \qquad 2.15$$

$$= \frac{\phi}{\tau} \frac{\partial f_o}{\partial E} \qquad 2.16$$

It is assumed that $\nabla_{\vec{r}} f \approx \nabla_{\vec{r}} f_o$, and the following relations apply:

$$\nabla_{\vec{r}} f_o = \frac{\partial f_o}{\partial T} \nabla_{\vec{r}} T \qquad 2.17$$

and:

$$\frac{\partial f_o}{\partial T} = -\frac{E-E_F}{T}\frac{\partial f_o}{\partial E} - \frac{\partial E_F}{\partial T}\frac{\partial f_o}{\partial E} \qquad 2.18$$

From the Fermi-Dirac distribution. Then $\phi$ in equation 2.16 is given by

$$\phi = \tau[e\vec{\varepsilon} - (E - E_F)\nabla \ell n\ T] \cdot \vec{V} \qquad 2.19$$

The current density due to an external field in the x direction is given by:

$$J_x = -\frac{e}{4\pi^3} \int f(\vec{k}')\ V_x\ d\vec{k}' \qquad 2.20$$

In the presence of an electric field and a temperature gradient in the x direction $f(\vec{k})$ in equation 2.19 is equal to $\phi$. The current density can then be written:

$$J_x = \frac{e}{4\pi^3} \int -\tau e\varepsilon_x \frac{\partial f_o}{\partial E} V_x^{\,2}\, d\vec{k}' +$$

$$\int \tau(E - E_f + T\frac{\partial E_F}{\partial T})\ \nabla \ell nT\ V_x^{\,2} \frac{\partial f_o}{\partial E}\, d\vec{k}' \qquad 2.21$$

The transport integral $k_n$ is defined as:

$$k_n = -\frac{1}{4\pi^3} \int \tau\ V_x^{\,2}\ E^{n-1} \frac{\partial f_o}{\partial E}\, d\vec{k}, \text{ for } n = 1,2,3... \qquad 2.22$$

In terms of the transport integral equation 2.21 can be written:

$$J_x = k_1[e^2\varepsilon_x - eT\ \nabla\ (\frac{E_F}{T})] - k_2\ (\frac{e}{T})\ \nabla T \qquad 2.23$$

The measurement of the Seebeck coefficient requires that $J_x = 0$, therefore:

$$\varepsilon_x = \frac{1}{e}\ [\nabla E_F + (\frac{k_2}{k_1 T} - \frac{E_F}{T})\ \nabla T] \qquad 2.24$$

The Seebeck coefficient is defined as the ratio between the electric field and the temperature gradient. For electrons this is seen to be

$$\alpha_e = \frac{k_2 - E_F k_1}{e\, k_1\, T} \qquad 2.25$$

setting $\nabla E_F = 0$ in equation 2.24 due to steady state conditions. Using a gamma function approximation to the transport integrals $k_1$ and $k_2$, for which equal energy surfaces and a relaxation time approximation $\tau \propto E^{-s}$ are assumed, equation 2.25 can be written:[13,13]*

$$\alpha_e = -\frac{K}{e}\left[\left(\frac{5}{2} - S\right) + \frac{E_c - E_F}{KT}\right] \qquad 2.26$$

Equation 2.26 will be used in the interpretation of the Seebeck measurements below (see Section 2.2).

*This development is a summary of material found in these references.

## 2.2 Application to Semiconductors

The measured Seebeck voltage can be represented by:[1]

$$\Delta V_{n-cu} = \int_{o}^{T_1} \alpha_{Cu}\, dT + \int_{o}^{T_2} \alpha_{n}\, dT - \int_{o}^{T_2} \alpha_{Cu}\, dT \qquad 2.27$$

$$\Delta V_{n-Cu} = \int_{T_1}^{T_2} \alpha_{n}\, dT - \int_{T_1}^{T_2} \alpha_{Cu}\, dT \qquad 2.28$$

where $\alpha_{Cu}$ is the Seebeck coefficient of the copper thermocouple wires and $\alpha_{n}$ is the Seebeck coefficient of the film. The thermoelectric power is several orders of magnitude larger in semiconductors than in metals. In a metal, only a small number of free carriers are affected by the presence of a thermal gradient.[2] This contribution (due to the copper wires) to the Seebeck voltage is thus disregarded as it is not significant enough to effect the accuracy of the measurements. The Seebeck coefficient of the film is assumed to be the slope of $\Delta V$ vs $\Delta T$ as indicated later in Figure 7. Carrier concentrations can be found directly from the Seebeck measurements using equation 2.26:

$$\alpha = -86.3\ [(\frac{5}{2} - S) + \eta]\ (\frac{\mu V}{k}) \qquad 2.29$$

For n-type materials, $\eta$ has replaced $E_c - E_F/kT$ and is the distance (in units of kT) above or below the conduction band edge. The parameter "S" is determined by the transport properties within the grains of the film. The temperature difference should occur across the grains of the film rather than across the grain boundaries. The Seebeck coefficient

of a polycrystalline sample should be characteristic of the grains. For optical mode scattering the quantity $(\frac{5}{2} - S)$ varies between 1.8 and 2.4 with temperature (Figure 3) and is defined as A.[16] This mode of scattering has been assumed to be dominant in Bube and Chynoweth's work on sprayed $Zn_xCd_{1-x}S$[11] and in Bube's previous work with CdS films and single crystals.[9,10] For a non-degenerate semiconductor, $\eta << 0$, and Maxwell-Boltzmann statistics are valid. Thus, we can write:[17]

$$\ell n \frac{N_c}{n} = \frac{E_c - E_F}{kT} = \eta \qquad 2.30$$

where $N_c$ is the density of states in the conduction band and n is the carrier concentration. The Seebeck equation thus becomes:

$$\alpha = -86.3 \left[\ell n \frac{N_c}{n} + A\right] \left(\frac{\mu V}{k}\right) \qquad 2.31$$

where A is the quantity specified in Figure 3. As the Fermi energy approaches the conduction band edge and crosses it (as the material becomes degenerate), classical statistics are no longer valid. According to Maxwell-Boltzmann statistics, all electrons have zero energy at 0K. In actuality, the electrons follow the Fermi-Dirac distribution function:

$$f_o(E) = \frac{1}{\exp\left[\frac{E-E_F}{kT}\right] + 1} \qquad 2.32$$

which more closely approximates the distribution of electrons when $\eta \geq 0$. This is true because as a material becomes more degenerate every electron does not have an opportunity to readjust to thermal change due to the increased number of electrons in energy levels

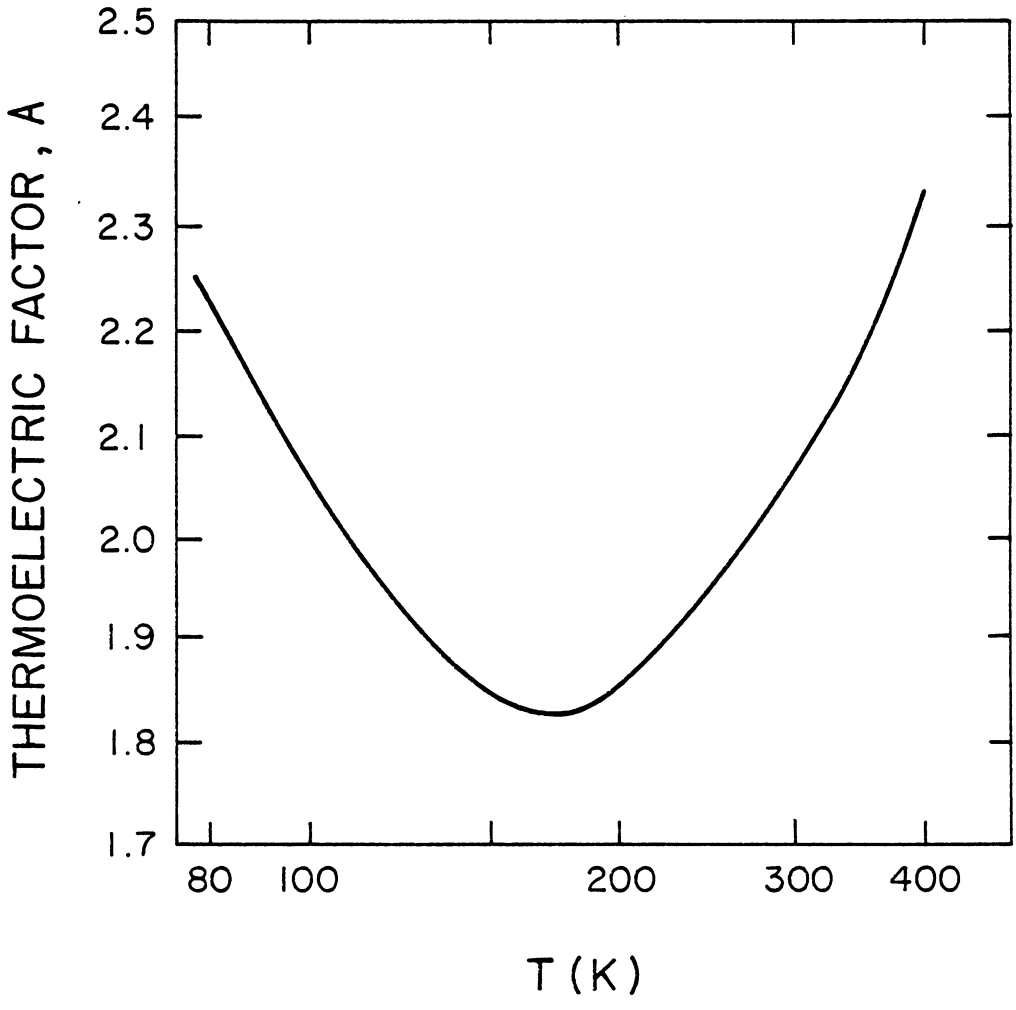


Figure 3. The thermoelectric factor A versus temperature.

directly above and below.

The number of electrons in the conduction band is given by:[18]

$$n = \int_{E_c}^{\infty} f_o(E)\, g(E)\, dE \qquad 2.33$$

where $g(E)$ is the density of energy states and $f_o(E)$ is the probability of finding an electron in a state of energy E (given by equation 2.32). The density of states is given by:[17]

$$g(E) = 4\pi\left(\frac{2m^*}{h^2}\right)^{3/2} (E - E_c)^{1/2} \qquad 2.34$$

where $m^*$ is the effective mass of the electron within the crystal.

Combining Equations 2.32, 2.33 and 2.34:

$$n = \int_{E_c}^{\infty} \frac{4\pi\left(\frac{2m^*}{h^2}\right)^{3/2} (E-E_c)^{1/2}}{1 + \exp\left(\frac{E-E_F}{kT}\right)}\, dE \qquad 2.35$$

Defining:

$$\varepsilon = \frac{E-E_c}{kT} \qquad 2.36$$

and

$$\eta = \frac{E_F-E_c}{kT} \qquad 2.37$$

Equation 2.35 can be written:

$$n = 4\pi\left[\frac{2m^*kT}{h^2}\right]^{3/2} \int_o^{\infty} \frac{\varepsilon^{\frac{1}{2}}\, d\varepsilon}{(1 + \exp(\varepsilon-\eta)} \qquad 2.38$$

in simplified form this can be written:

$$n = N_c\, F_{\frac{1}{2}}(\eta) \qquad 2.39$$

where $N_c$, the density of states, has been defined as:

$$N_c = 4\pi \left[ \frac{2m^* kT}{h^2} \right] \qquad 2.40$$

and the Fermi-Dirac integral is defined as:

$$F_i(\eta) = \frac{1}{\Gamma(i+1)} \int_0^\infty \frac{\varepsilon^i}{1+\exp(\varepsilon-\eta)} \, d\varepsilon \qquad 2.41$$

The density of states ($N_c$) is found using effective mass ratios of .33[19] for silicon and .25[10] for CdS and ZnCdS film samples. For $0 \leq \eta \leq 1.3$, the Fermi-Dirac integral was approximated by:[18]

$$F_{1/2}(\eta) = \frac{\exp(\eta)}{1+0.27\exp(\eta)} \qquad 2.42$$

This approximation lies within ± 3% of $F_{1/2}(\eta)$ in this range. The approximation:

$$F_{1/2}(\eta) = \left( \frac{4\eta^{3/2}}{3\pi^{1/2}} \right) \left[ 1 + \frac{\pi^2}{8\eta^2} \right] \qquad 2.43$$

is useful in the range $1.5 \leq \eta \leq 5$.[18] This approximation also lies within ±3% of $F_{1/2}(\eta)$ in this range. The approximations were used in determining the carrier concentrations in the 3 μm and the 9.3 μm CdS films. Classical statistics were used in determining the carrier concentrations in all other samples.

## III. Experimental Procedure

### 3.1 The Seebeck Apparatus

The apparatus for making Seebeck measurements was designed for both accuracy and simplicity (Fig. 4). The Seebeck voltage was measured directly from the copper thermocouple wires on a Keithly 174 digital multimeter in the case of a high resistance film ($> 10^5$ Ω) and on a Keithly 160B digital multimeter in the case of a lower resistance film ($< 10^5$ Ω). The Keithly 174 was used on the higher resistance films because its higher input impedance ($10^9$ Ω in the mV range) resulted in greater accuracy. The thermocouples were placed directly on the film surface. A gallium-indium eutectic alloy was painted on two edges of the film, and the thermocouples were secured mechanically onto the painted portions by means of brass screws, as shown. This insured good ohmic contact between the thermocouple and the film. An Omega 400A digital thermometer was used to measure the temperature at the points on the film under the two screws. A two throw three pole switch was used to connect the circuit between the digital thermometer and the thermocouples so both temperatures could be easily measured. The constantan thermocouple wires were connected to a Keithly 225 current source in order to obtain the constant D.C. current needed to make resistance measurements (Fig. 5).

The Seebeck coefficients were determined on the various films over a temperature range of -180C to room temperature. These temperatures were obtained by a combination of liquid nitrogen cooling and heating with two 5 watt "Hotwatt" heaters $\frac{1}{8}$" in diameter and 1" long.

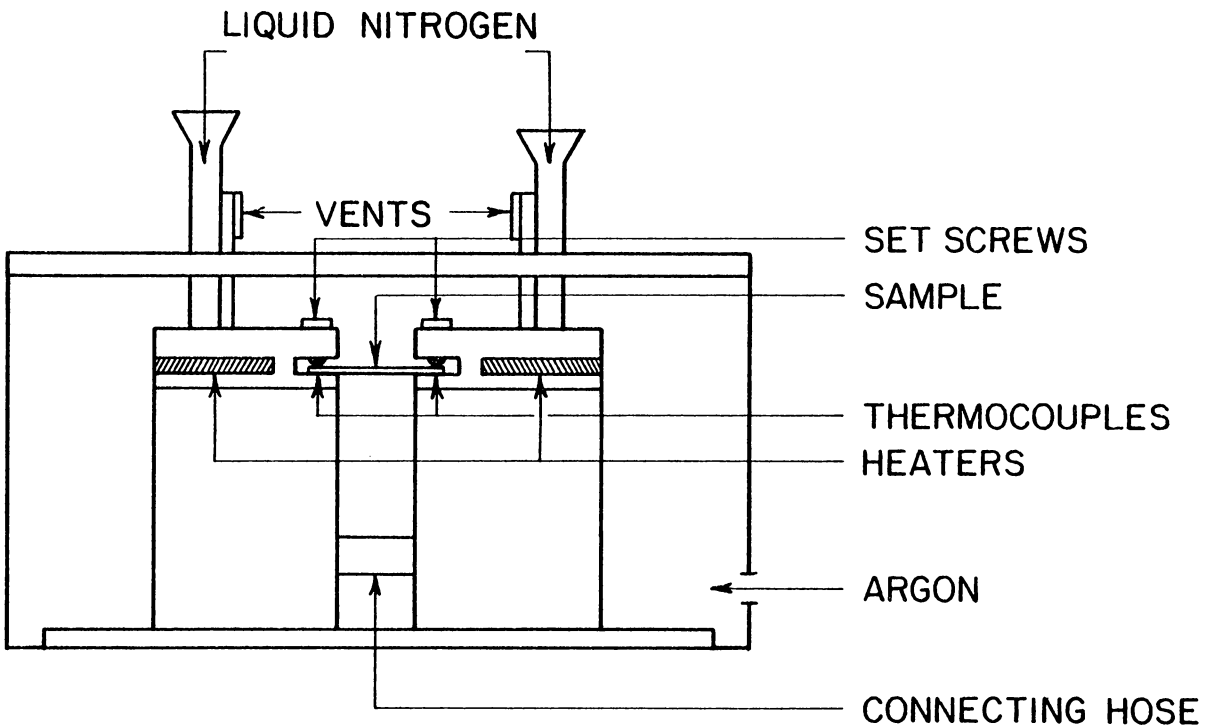


Figure 4. Apparatus for making Seebeck measurements on thin films.

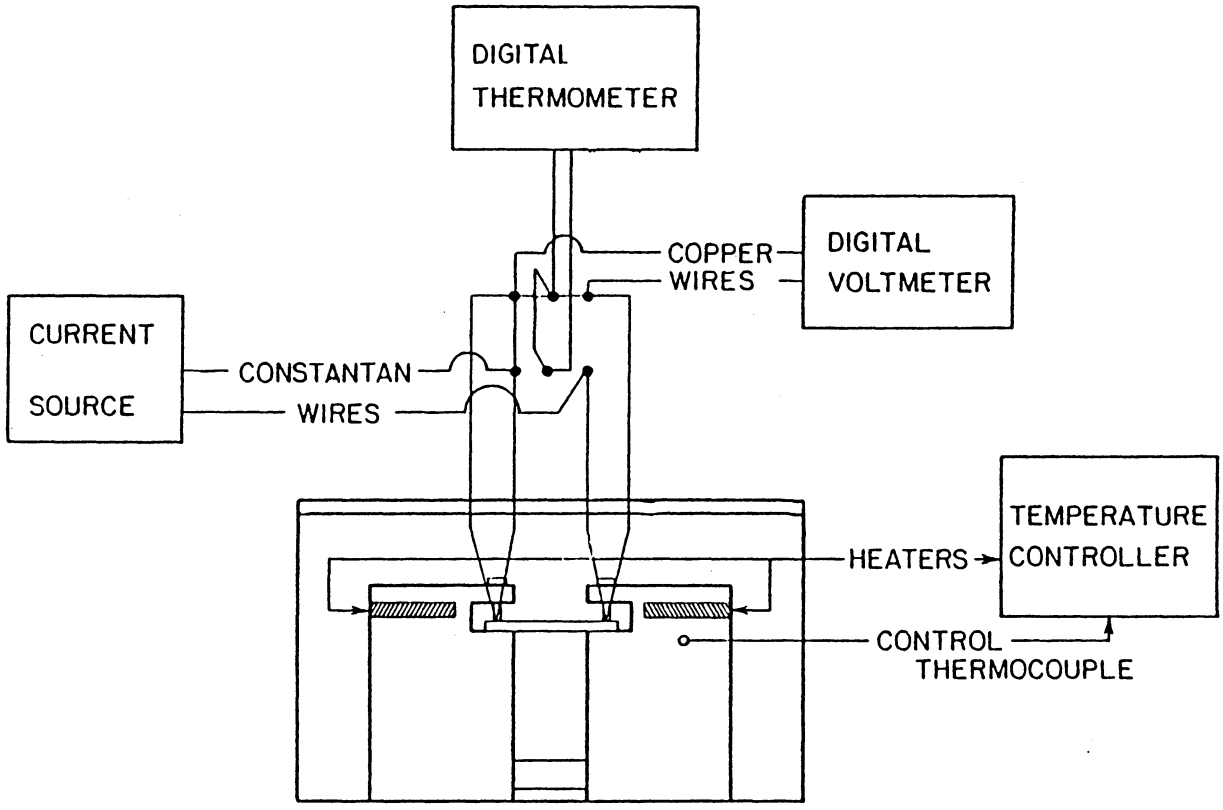


Figure 5. Circuit diagram for Seebeck effect and electrical resistivity measurements.

The heaters were controlled by an Omega 49 proportioning temperature controller. The control thermocouple was placed on the surface of the left liquid nitrogen cylinder (Fig. 5). The liquid nitrogen was fed into the copper cylinders through two $\frac{1}{4}$" copper tubes with funnels attached at the top. Vents also made of $\frac{1}{4}$" copper tubing were placed in the top of the copper cylinders behind the feed lines. The two copper cylinders were made from a 1½" diameter copper rod. The rod was cut into two 2½" long sections (Fig. 6). The top ½" was then cut from each of these sections to be used as a cap. The bottom 2" sections were milled to a depth of $1\frac{3}{4}$" at a diameter of 1". This left a thickness of ¼" along the sides and on the bottom of the cavity. A $\frac{1}{8}$" slot was placed $\frac{3}{8}$" into each of the caps $\frac{1}{8}$" from the bottom. Set screws were placed through the tops of the caps over the slots for mounting the sample between the two copper cylinders. A $\frac{1}{8}$" diameter 1" deep hole was drilled into each of the caps directly opposite from the slots for mounting heaters. Two ¼" holes were drilled in each cap for the intake and vent tubing. A ¼" diameter plastic tube was placed between the two cylinders to allow liquid nitrogen to flow between the two cylinders. This insured that the temperature gradient between the ends of the sample would be relatively small ($< 15^{o}C$). The connecting hose was made of an electrical insulator so that an open circuit existed, and the Seebeck voltage could be measured across the sample.

The two copper cylinders were mounted on a 5" X $2\frac{3}{4}$" X ½" Lucite plate with epoxy. The caps were mounted onto the cylinders with silicone epoxy. The apparatus was placed in a box 5" X 6" X 3" made

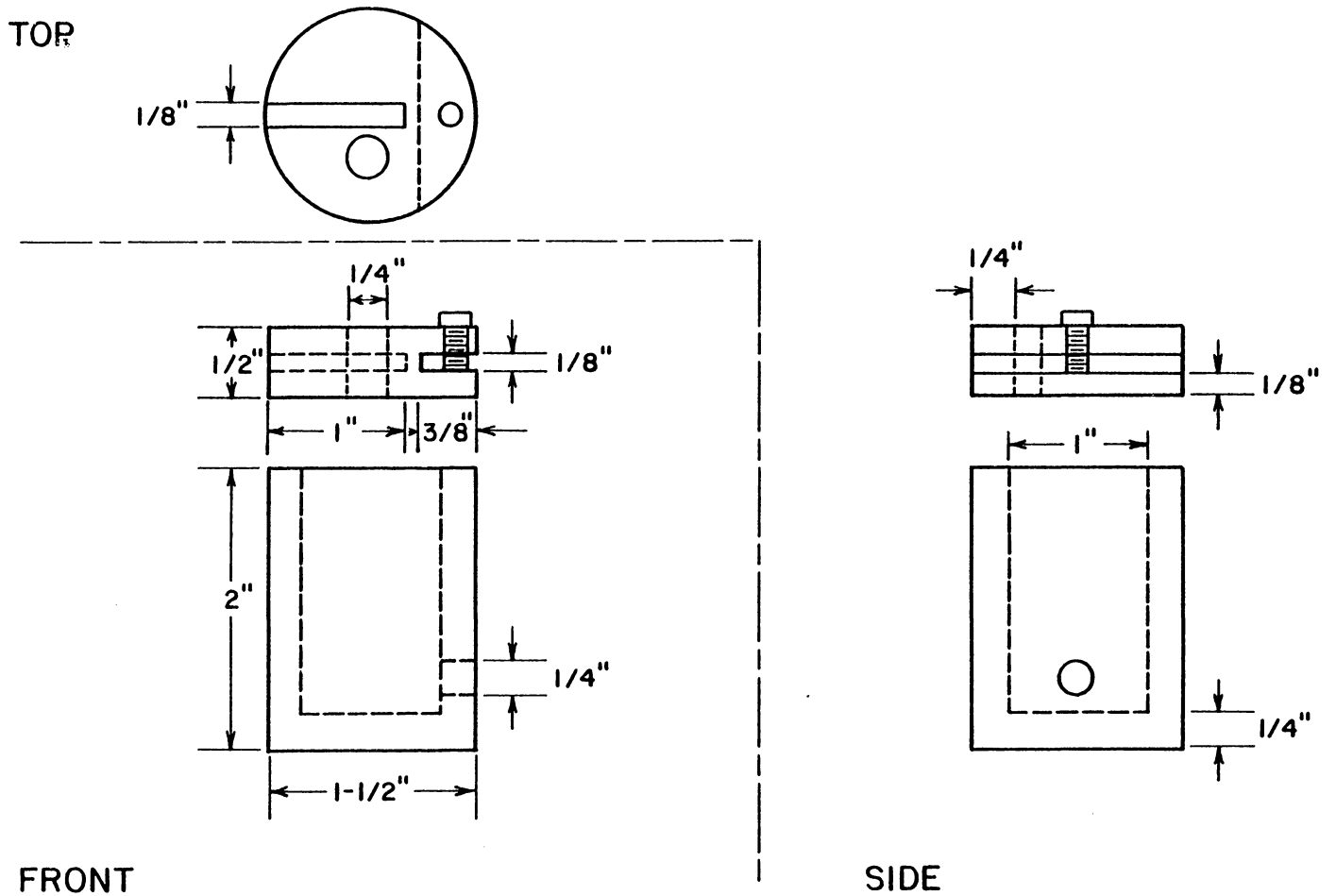


Figure 6. Thin Film Sample Holders.

of ¼" thick Lucite with ¼" diameter holes drilled for the feed and vent tubes. This prevented excess liquid nitrogen from interferring with the measurements. The box was purged with argon before liquid nitrogen was added to keep water vapor from condensing on the sample during measurements. The cylinders and copper tubing were insulated with cotton cloth to help keep frost from forming on the outside of the lucite box. This was to allow for the observation of the sample during the low temperature measurements.

## 3.2 Sample Preparation

CdS and ZnCdS films were all vapor deposited onto glass. Table I shows a summary of the samples. The films were deposited in a Denton DV-503 high vacuum evaporator. The vacuum pressure during the depositions was typically $10^{-6}$ Torr, and the time of deposition (thickness) was controlled by a shutter which prevented the evaporated species from reaching the substrate when closed. Two glass substrates were used in each deposition. Substrate temperatures used during the depositions and resulting film thicknesses are also shown in Table I.

Table I. Summary of CdS and $Zn_xCd_{1-x}S$ Samples.

| Sample # | Composition | Substrate Temperature (°C) | Thickness (μm) |
|---|---|---|---|
| 1 | Silicon* | | |
| 2-1 | CdS | 100 | 1.5 |
| 2-2 | CdS | 200 | 1.7 |
| 2-3 | CdS | 100 | 3.0 |
| 2-4 | CdS | 200 | 3.0 |
| 2-5 | CdS | 200 | 9.3 |
| 2-6 | CdS | 200 | 14.0 |
| 3-1 | $Zn_{.04}Cd_{.96}S$ | 200 | 16.6 |
| 3-2 | $Zn_{.15}Cd_{.85}S$ | 200 | 17.0 |

*Single Crystal Sample

3.3 Seebeck Measurements

Seebeck measurements were made on each of the films at room temperature. If the film was measurable (a resistance lower than $10^7$ Ω and a Seebeck voltage greater than .1 mV for a $10^{o}$C temperature gradient) then the measurements were extended to between -180$^{o}$C and room temperature.

The room temperature measurement was made by heating up one side of the sample while leaving the other at room temperature. The Seebeck voltage was measured at various temperature gradients from 3$^{o}$C to 12$^{o}$C. When the voltage versus the temperature gradient was plotted a linear relationship was found as expected from equation 1.1 (Fig. 7). The slope of the line is the Seebeck coefficient at room temperature. In all cases the measured value of the Seebeck coefficient was assumed to occur at the average of the two end temperatures.

After the room temperature measurement was completed, liquid nitrogen was added to both sides of the Seebeck apparatus. A natural temperature difference of about 15$^{o}$C was found to exist upon cooling. This was probably due to the differences in venting and insulation between the two sides of the apparatus. The temperature was allowed to stabilize at intervals of approximately 25$^{o}$C. At each interval the gradient was controlled by the heater in one of the copper cylinders and was maintained between 4$^{o}$C and 8$^{o}$C for most measurements. A larger gradient was used if the Seebeck voltage was small ($< .2$ mV) but was still kept less than 12$^{o}$C. A number of readings were made at each temperature. The averages of the Seebeck coefficients calculated at each interval were used in the final plots.

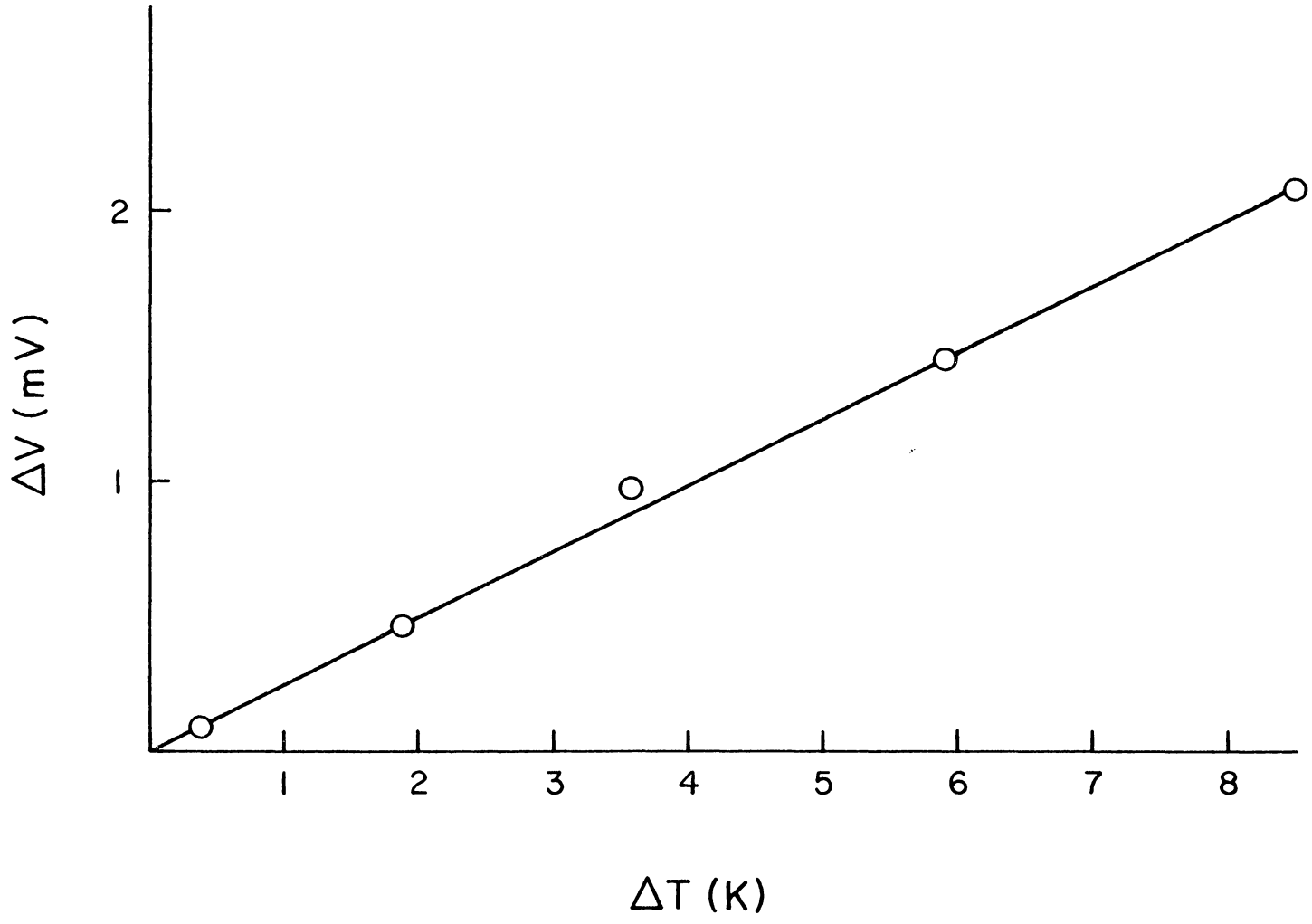


Figure 7. Room temperature measurements of the Seebeck Effect in thin film CdS.

## 3.4 Electrical Resistivity Measurements

The Seebeck apparatus was also used to measure the electrical resistivity of the thin film and single crystal samples. The sheet resistance was measured across a square section of film as a function of temperature. The measurements were made at 25°C intervals starting near liquid nitrogen temperature (-180°C) and ending at room temperature. The temperature gradient between the two ends of the sample was kept to a minimum using the heaters and controller. An average of the two temperatures was used in the final plot. The resistance was measured by applying a D.C. current across the constantan thermocouple wires and measuring the voltage developed across the copper thermocouple wires. The resistivity was found by dividing the measured sheet resistance by the thickness of the film. Film masses were determined by weighing the samples before and after dissolving the films in a dilute HCl solution. The volume of film present on the substrate was calculated using the theoretical density of hexagonal CdS (4.82 $gm/cm^3$). The Zn content in the $Zn_xCd_{1-x}S$ films was found by atomic absorption and x-ray measurements.

3.5 Hall Measurements

The van der Pauw method[14] was used to measure the room temperature Hall voltage. The four leads needed to make the measurements were attached to the film surface with a gallium-indium eutectic compound at the four corners of the sample (Figure 8). The resistance was measured using the configuration shown in Figure 8. The resistance is given by:

$$R_a = V_{12}/I_{34} \tag{3.1}$$

where $V_{12}$ and $I_{34}$ are voltage and current for the leads as shown. The resistance must also be measured in the other direction. This is given by:

$$R_b = V_{23}/I_{41} \tag{3.2}$$

The sheet resistance can be found by:

$$\rho = \frac{\pi}{\ell n 2}\left(\frac{R_a + R_b}{2}\right) f\left(\frac{R_a}{R_b}\right) \tag{3.3}$$

where $f\left(\frac{R_a}{R_b}\right)$ is the correction function shown in Figure 9. The Hall resistance $\Delta R_e$ is found using the configuration in Figure 8 (b) and is the change in the resistance when a magnetic field is applied perpendicular to the sample, as follows:

$$\Delta R_e = V_{13}/I_{42}\Big|_{B=0} - V_{13}/I_{42}\Big|_{B=N} \tag{3.4}$$

The mobility is given by:[14]

$$\mu = 10^8(\Delta R_e t/B\rho)\left(\frac{cm^2}{volt \cdot sec}\right) \tag{3.5}$$

and the carrier concentration can be found from

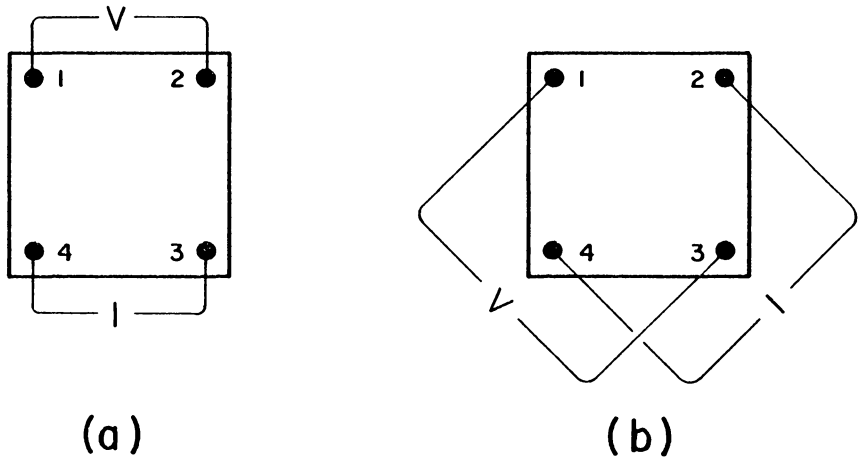


Figure 8. Current-Voltage configurations for measuring (a) sheet resistance and (b) Hall voltage on a thin film sample using the van der Pauw method.

$$n = \frac{1}{\rho e \mu} \qquad 3.6$$

A current of about 2 mA was used, and voltages between 0.1 and 0.3 volts were measured. The Hall voltage ($V_{13}$) was measured using a 12.7 kgauss magnetic field normal to the film plane. The voltage was recorded on a strip chart recorder for both directions of the magnetic field. The current used in the Hall measurements was also about 2 mA. The strip chart recorder was zeroed with no magnetic field being applied to the sample (see Figure 9).

Voltage measurements were then made with the magnetic field applied. A number of measurements were made on each film, and the average was used to find the Hall mobility.

Resistivity measurements are used with the carrier concentration results to find the drift mobility according to equation 1.3. The change in drift mobility with temperature gives an indication of the dominant scattering mechanism. Grain boundary scattering is described by the Petritz theory discussed in Chapter 1. Other types of scattering mechanisms are optical and acoustic modes of phonon scattering, scattering due to charged and neutral imperfections, dislocations, and inhomogeneities.

Hall measurements are made to compare drift mobility values found from Seebeck measurements with Hall mobility values. These values should be similar although they are not exactly equal because the transport properties are changed by the magnetic field used in Hall measurements.

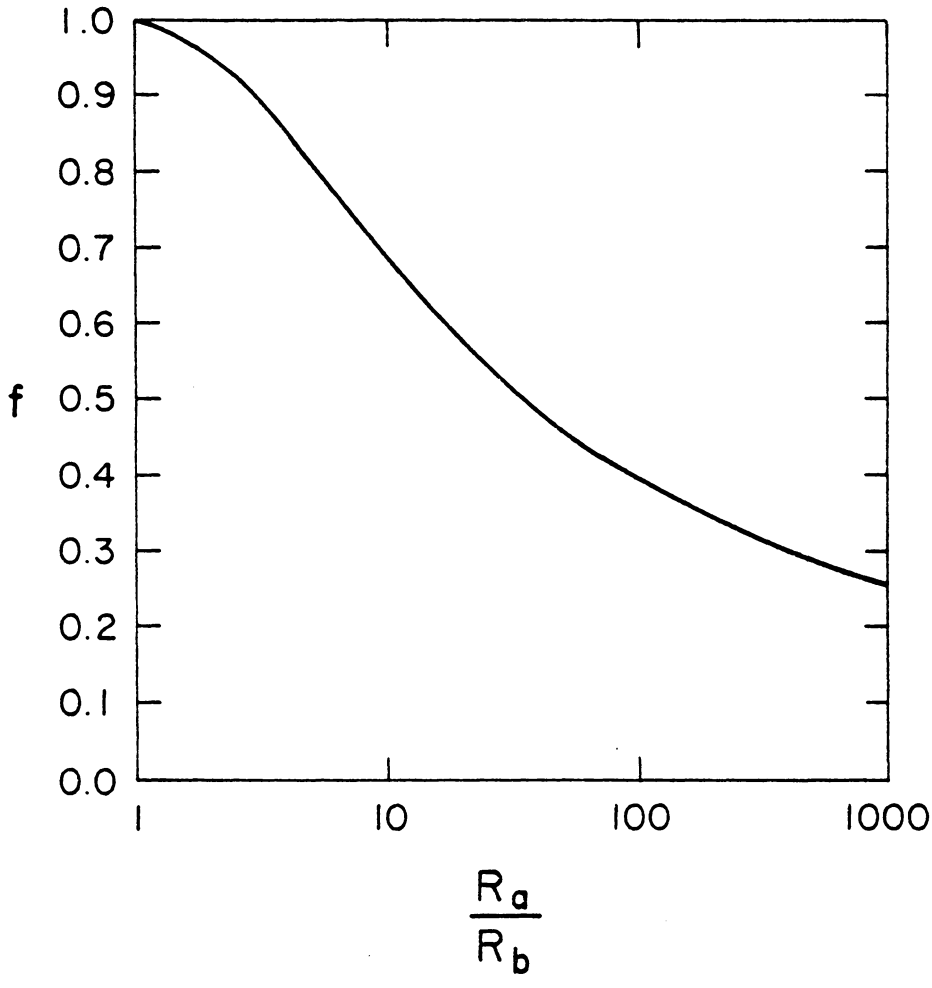


Figure 9. Van der Pauw Correction Function.

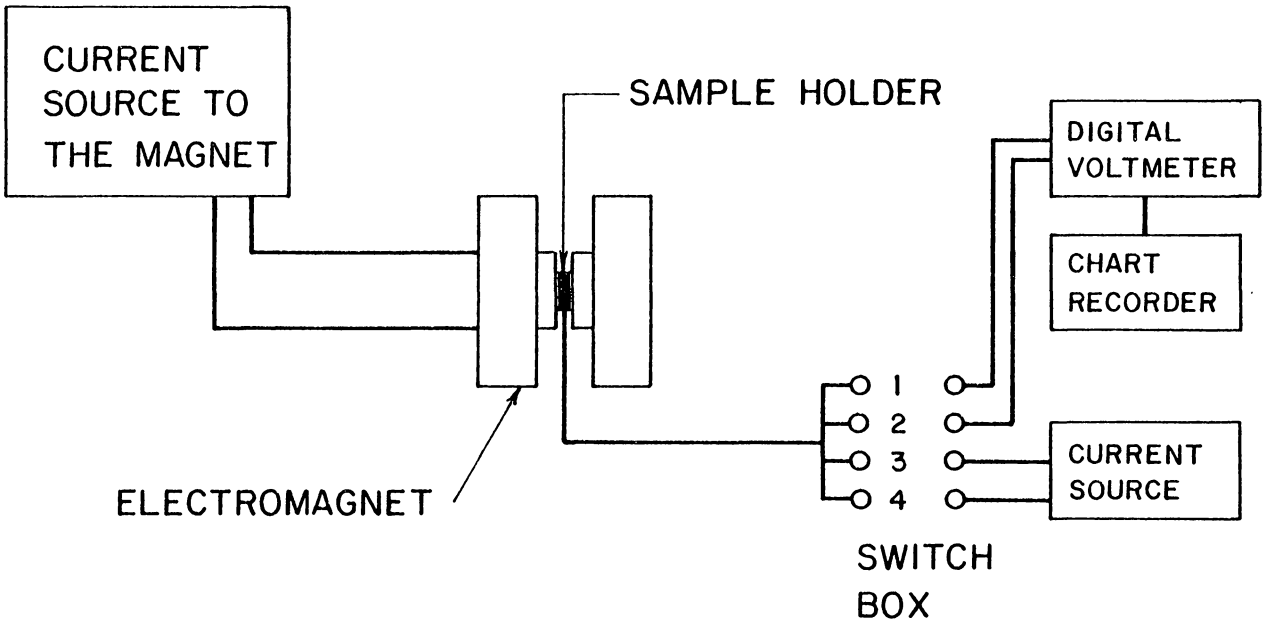


Figure 10. The Hall Effect Apparatus.

## IV. Results and Discussion

### 4.1. Silicon Standard

An n-type single crystal silicon wafer (.005 Ω-cm) was used to test the accuracy of the Seebeck apparatus. A room temperature value of -.707 mV/k was found for the Seebeck coefficient. The Seebeck coefficients of heavily doped n-type silicon samples were measured by Brinson and Dunstan.[19] A value of -.650 mV/k was found for a silicon sample with a resistivity of .005 Ω-cm. The mobility in the silicon standard sample is found to be $6.5X10^{2}$ $cm^{2}$/volt·sec.

### 4.2. Effect of Film Thickness for CdS Films

Measurements were made on six CdS film samples. A summary of room temperature results are in Table II. Seebeck measurements were not made on samples 2-1, 2-2, and 2-3 because of high film resistances. Seebeck data for films 2-4, 2-5, and 2-6 can be found in Figures 11, 12 and 13, respectively. Room temperature values of the Seebeck coefficients range from -.040 $(\frac{mV}{^{o}K})$ in the 3 μm thick sample to -.255 $(\frac{mV}{^{o}K})$ in the 14 μm thick sample. These correspond to carrier concentrations of between $1.05X10^{18}$ to $4.25X10^{18}$ $cm^{-3}$ in the 14 μm thick and 3 μm thick sample, respectively. The sign of the Seebeck coefficient indicates that the samples are n-type as expected. A slightly higher carrier concentration is seen in the thinner films which could be due to several mechanisms: 1) larger defect and trap density in thinner films could be electrically active as donor levels, 2) impurities from the substrate which act as

TABLE II. Summary of CdS Film Results (Room Temperature)

| Sample | Thickness (μm) | ρ(Ω-cm) | $\alpha(\frac{mV}{^oK})$ | $n(cm^{-3})$ | $\mu(\frac{cm^2}{volt \cdot sec})$ |
|---|---|---|---|---|---|
| 2-1 | 1.5 | $1.65X10^7$ | - | - | - |
| 2-2 | 1.7 | $1.02X10^7$ | - | - | - |
| 2-3 | 3.0 | $6.88X10^6$ | - | - | - |
| 2-4 | 3.0 | $3.06X10^3$ | -.040 | $4.25X10^{18}$ | $.73X10^{-3}$ |
| 2-5 | 9.3 | 2.89 | -.158 | $1.96X10^{18}$ | 1.1 |
| 2-5 Hall | 9.3 | 2.89 | - | $2.44X10^{18}$ | .886 |
| 2-6 | 14.0 | 4.27 | -.255 | $1.05X10^{18}$ | 2.7 |

ρ = electrical resistivity

α = Seebeck coefficient

n = electron concentration

μ = electron mobility

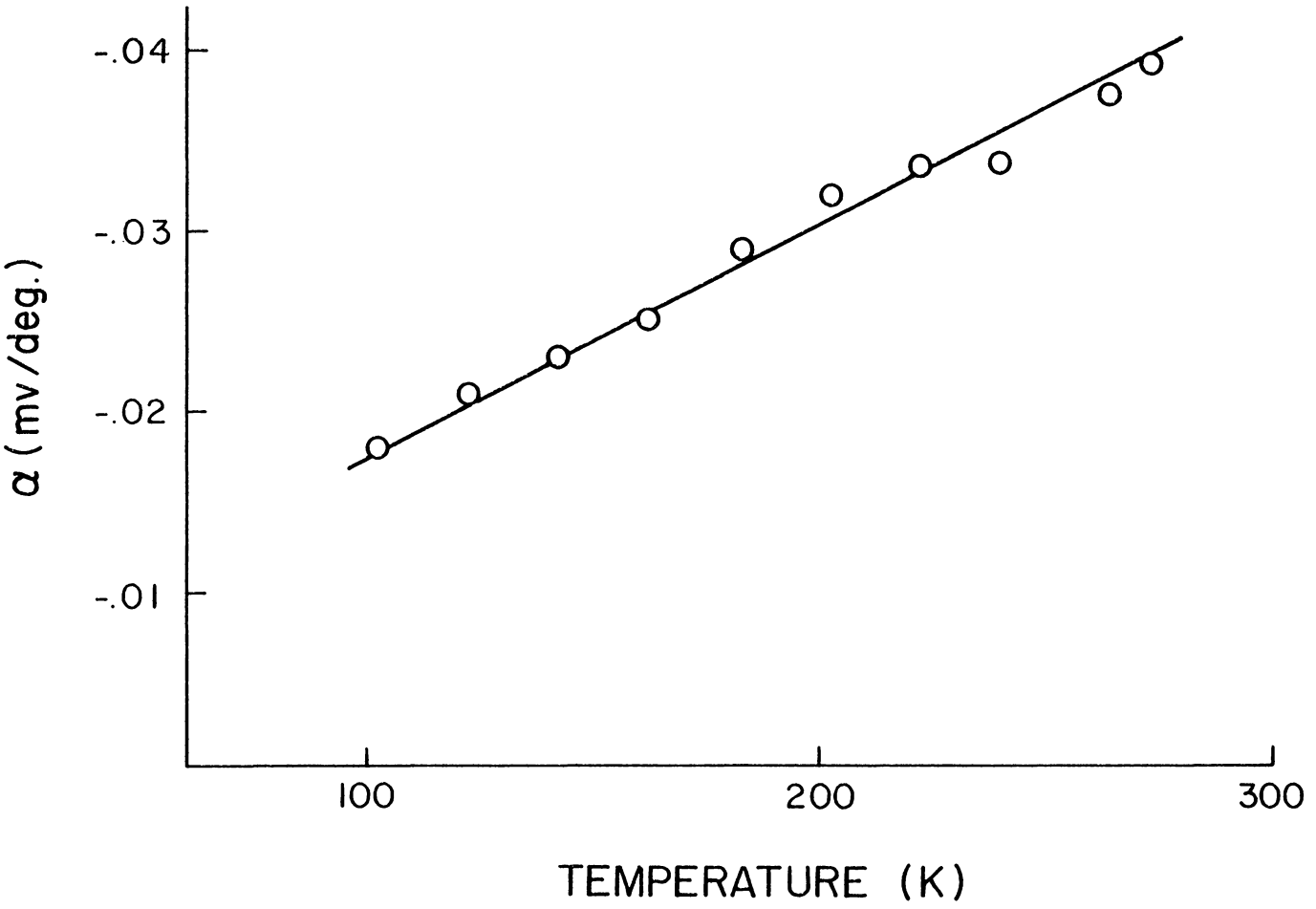


Figure 11. The Seebeck coefficient versus temperature for the 3.0 μm CdS film.

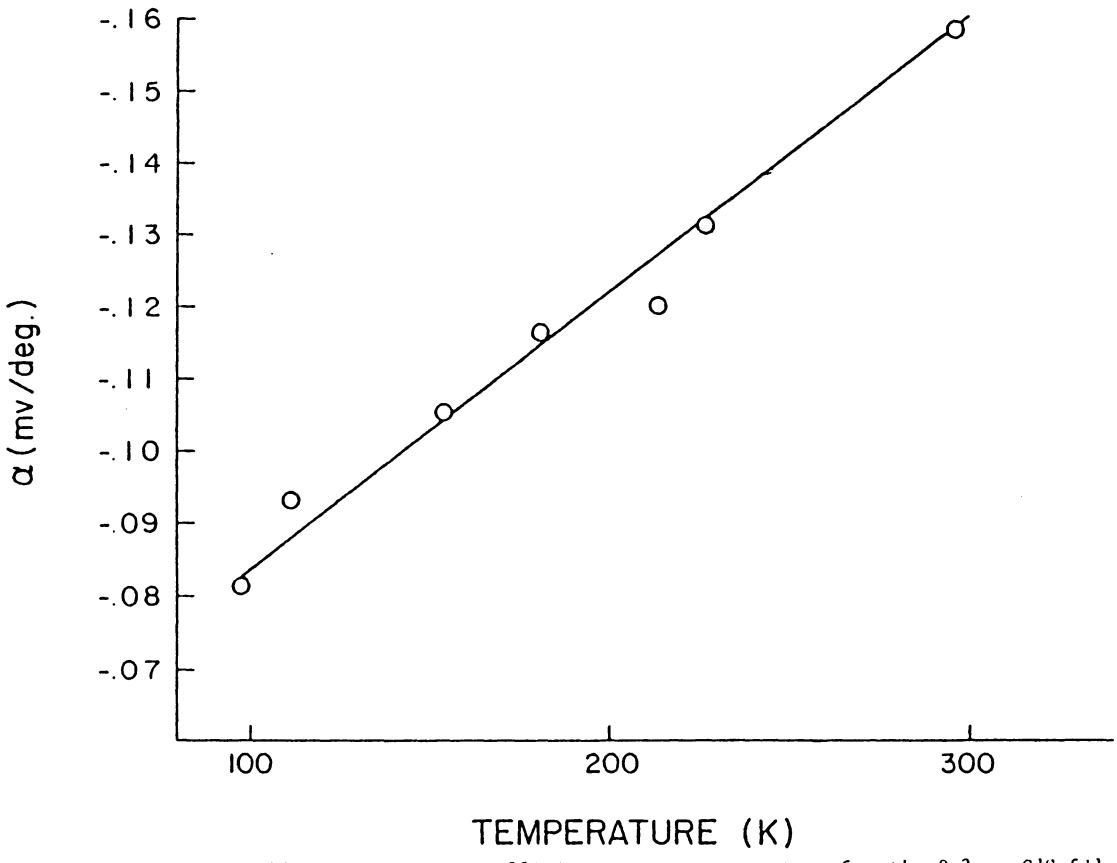


Figure 12. The Seebeck coefficient versus temperature for the 9.3 μm CdS film.

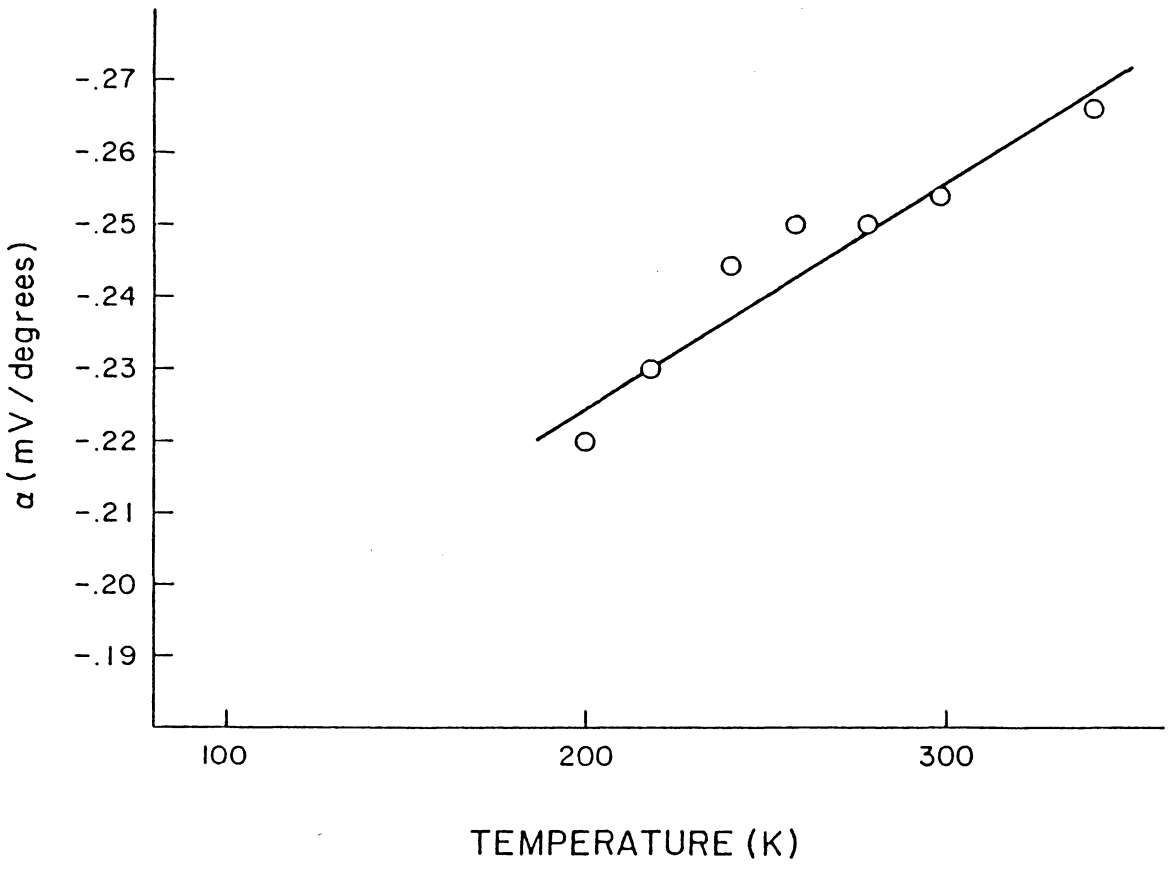


Figure 13. The Seebeck coefficient versus temperature for the 14.0 μm CdS film.

donors would be more likely to effect a thinner film, and 3) a Cd rich film would be more likely at the early stage of deposition due to the preferential sublimation of cadmium over sulfur. Equation 2.42 was used to approximate the Fermi-Dirac integral for the 9.3 μm film which had $\eta$ values of between .169 and 1.06 at temperatures between 296 K and 98 K respectively. The approximation given by equation 2.43 was used in finding carrier concentration values for the 3 μm film. This film has $\eta$ values between 1.55 and 1.79 at temperatures ranging from 273 K to 103 K. Classical statistics were used in finding the carrier concentration in the 14 μm film. The Fermi level was well below the conduction band edge over the entire temperature range. In polar semi-conductors, such as metallic oxides and sulfides, the optical branch of lattice vibrations is often the predominant scattering mechanism. The optical mode of scattering is assumed predominant in all films; thus the quantity $(\frac{5}{2} - S)$ was set equal to the thermoelectric factor A given in Figure 3.

The variance in resistivity with temperature for the 3 μm, 9.3 μm, and 14 μm films are shown in Figures 14, 15, and 16, repsectively. The room temperature resistivity increased with decreasing film thickness from 4.27 Ω-cm in the 14 μm film to $1.65 \times 10^7$ Ω-cm in the 1.5 μm film. The increase in resistivity is directly related to a decrease in carrier mobility according to equation 1.3. The resistivity of $\sim$ 1.5 μm films and of 3.0 μm films decreased as the substrate temperature (upon deposition) is increased (from 100°C to 200°C) from $6.88 \times 10^6$ to $3.06 \times 10^3$ in the 3 μm films and from $1.65 \times 10^7$ to $1.02 \times 10^7$ in the 1.5 μm films. As the substrate temperature is increased, the evaporated

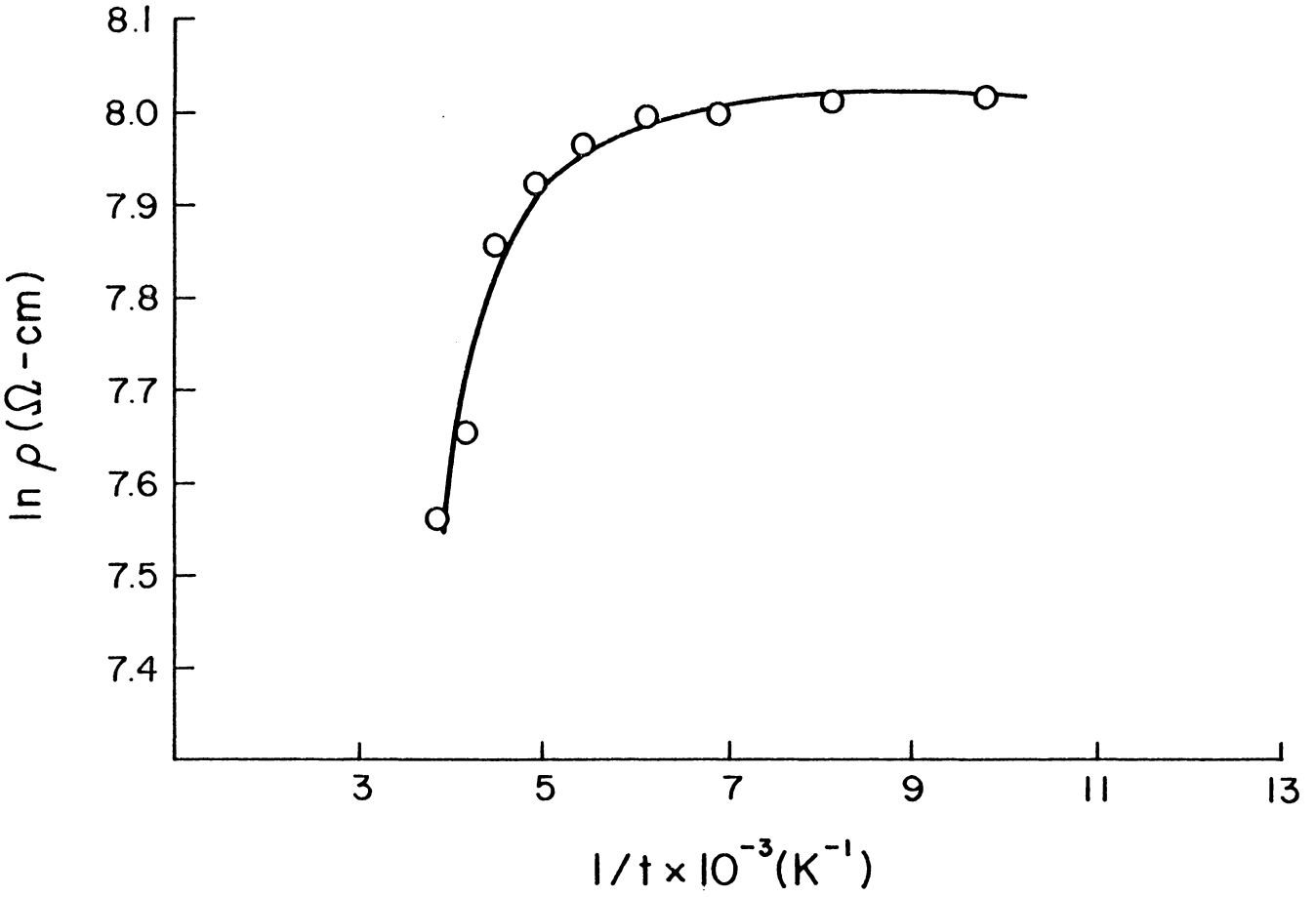


Figure 14. Resistivity versus inverse temperature for the 3.0 μm CdS film.

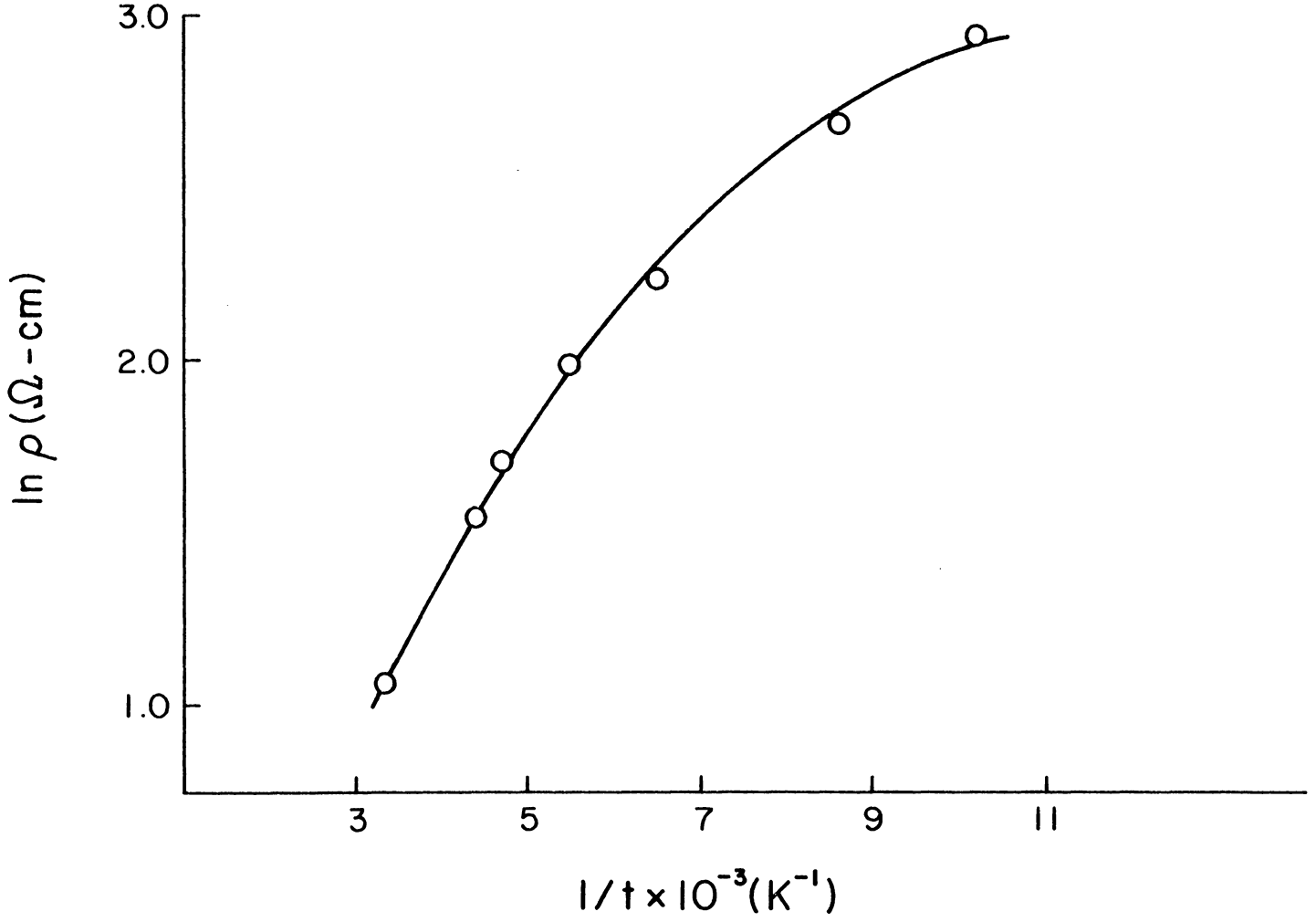


Figure 15. Resistivity versus inverse temperature for the 9.3 μm CdS film.

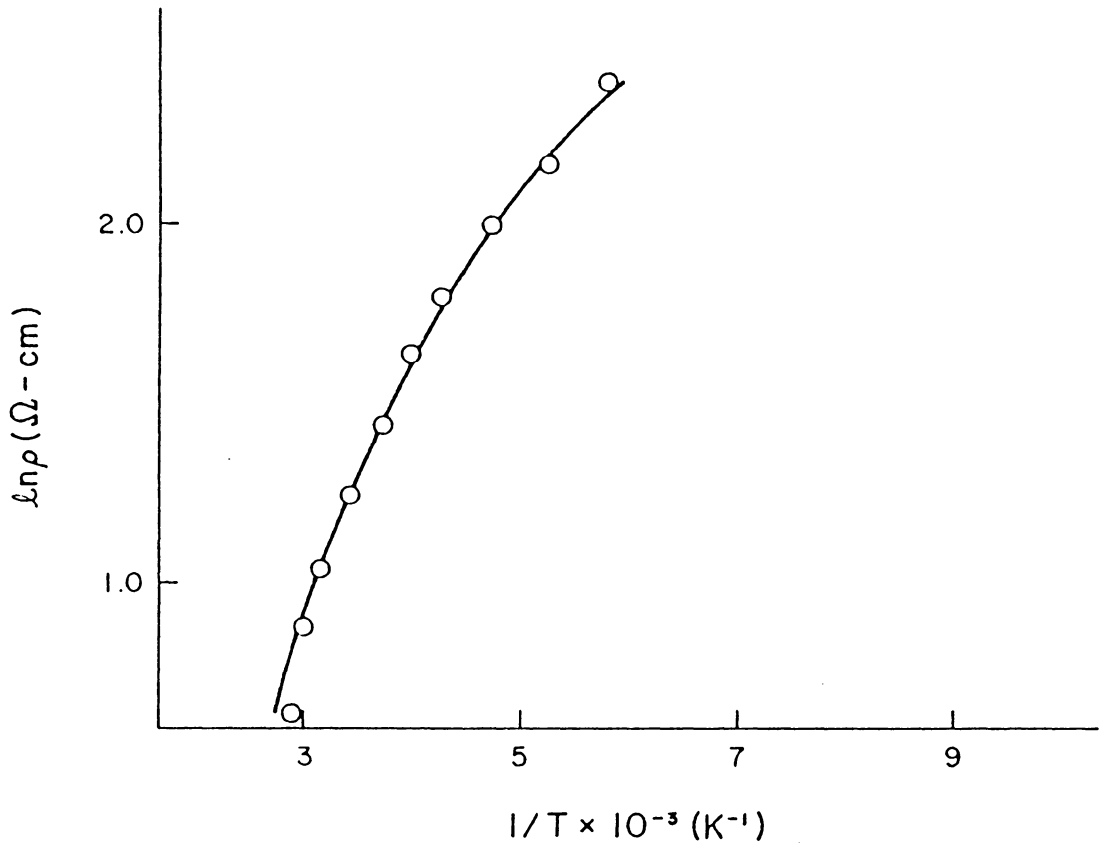


Figure 16. Resistivity versus inverse temperature for the 14.0 μm CdS film.

species will have a greater amount of mobility as they land on the substrate. This allows the atoms to arrange themselves in the configuration of lowest energy, i.e. a state of increased crystallinity. Scattering due to inhomogeneity is decreased with increased crystallinity and mobility is increased. Thus, the resistivity of the film goes down. The variation in resistivity with temperature follows the results given by Bleha et al.[21] for vacuum deposited CdS films. The activation energy for electrical conduction was not calculated because the linear region does not fall within the temperature range for which electrical resistivity measurements were made in these films.

The room temperature mobility increases from $0.73X10^{-3}$ $cm^2/volt \cdot sec$ in the 3 μm film (200°C substrate temperature) to 2.7 $cm^2/volt \cdot sec$ in the 14 μm film. This increase is due to several mechanisms. First, chemisorption of oxygen creates a depletion layer near the surface of the film. This will have a greater effect in thinner films. Oxygen being electronegative and CdS being n-type, chemisorption occurs and oxygen atoms get fixed partly on sulphur vacancies. These atoms become trapping sites for free electrons.[22] The n-type nature of CdS is partly due to a high donor concentration at the surface caused by sulphur vacancies. Oxygen adsorption on the surface reduces the concentration of sulphur vacancies and thus the donor concentration.[23] The oxygen states are at energies well below that of the donor levels. They become acceptor states for free electrons.

Second, surface scattering due to localized surface states becomes more important in thinner films. These surface states are due to the

interruption of the periodicity of the lattice at the surface and because of the special chemical, atomic, and molecular properties of the surface atoms.[2]

Third, if a polycrystalline film is modeled as a collection of fine crystal grains with an average grain size of L separated by insulating intergranular regions of average thickness d the mobility will be dependent upon the ratio of L/d.[24] As the grains get smaller, as shown in Figure 17 for the 3 μm and 9.3 μm samples, the mobility will decrease because the average number of grain boundaries that must be crossed by an electron increases. Figure 18 shows the logarithm of n and μ versus the inverse of temperature. The ℓn n decreases linearly with the reciprical of temperature as expected, with the activation energy equal to .013 eV for the 14 μm and 9 μm samples and .018 eV for the 3 μm samples. The mobility is seen to be grain boundary dependent (according to equation 1.4) in the 14 μm and 9.3 μm films. The 14 μm film has a grain boundary activation energy of 0.0298 eV and a $\mu_o$ of 5.47 $cm^2$/volt·sec. The 9.3 μm film has a grain boundary activation energy of .0049 eV and a $\mu_o$ of 1.49 $cm^2$/volt·sec. As the carrier concentration of a polycrystalline film increases the effect of grain boundary scattering should decrease. The dangling bonds at the grain boundary behave as electron traps.[25] The barrier height can be calculated equating the depletion layer charge to the amount of charge accumulated in the interface states. As electrons are trapped the depletion layer charge decreases and free electrons move more easily across the grain boundary. A barrier height of 0.042 eV was reported

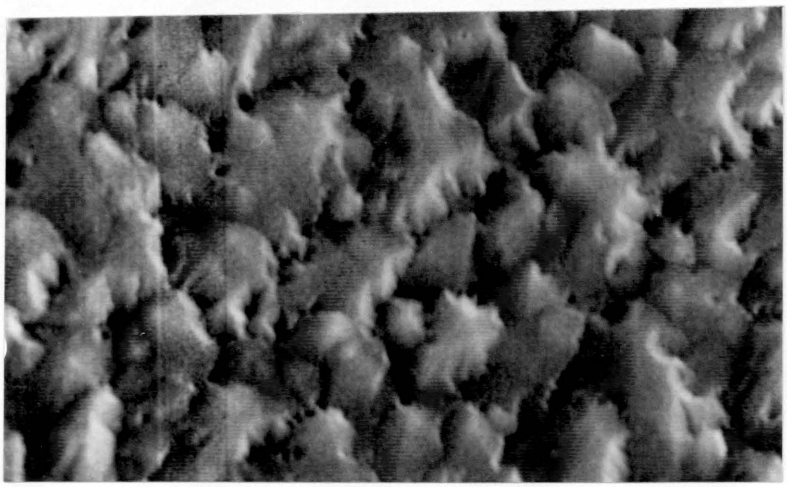

(a)

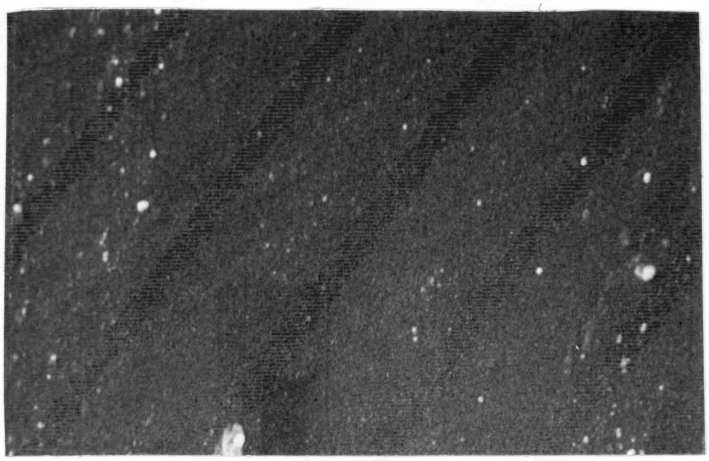

(b)

Figure 17. (a) In the 9.3 μm film (5000X) grains of an average diameter of 2.1 μm can be seen.

(b) In the 3.0 μm film (5000X) no grain structure can be seen.

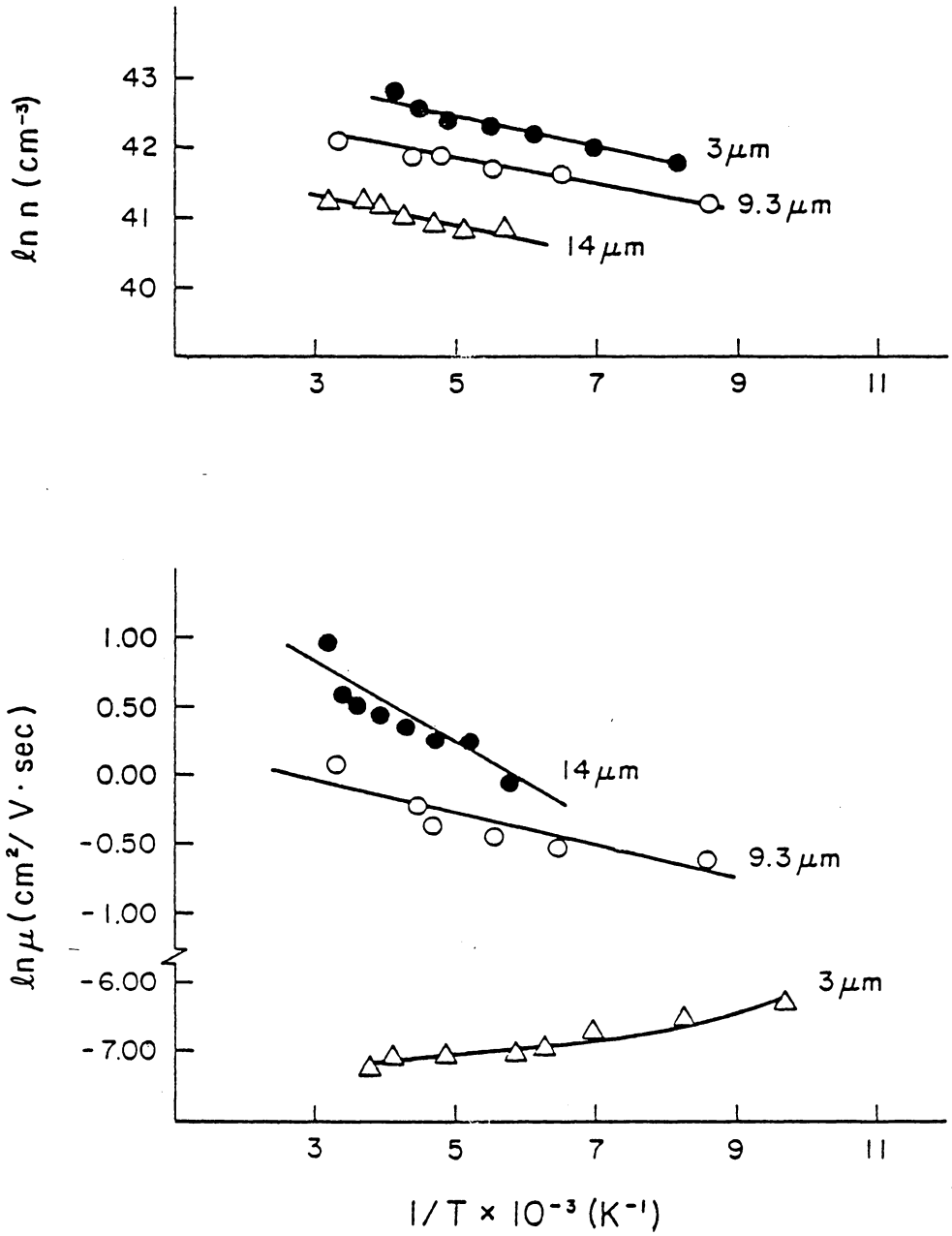


Figure 18. The logarithms of mobility and carrier concentration versus the inverse of temperature for the 3.0 μm, 9.3 μm, and 14.0 μm CdS films.

by Orton et al., for a CdS film with a carrier concentration of $1.7X10^{16}$ $cm^{-3}$.(4) The barrier height increased with decreasing carrier concentration to a value of 0.15 eV for a CdS film with a carrier concentration of $4.7X10^{14}$. The increasing degeneracy with decreasing film thickness causes a decreased dependence on grain boundary scattering in the 14 μm, 9 μm and 3 μm samples shown in Figure 18. The predominant scattering mechanism in the 3 μm film is lattice scattering in which mobility follows a $T^{-3/2}$ dependence (Figure 19). Hall measurements were made on the 9.3 μm CdS film. The results can be found in Table II. The values for mobility and carrier concentration closely match those found from Seebeck measurements.

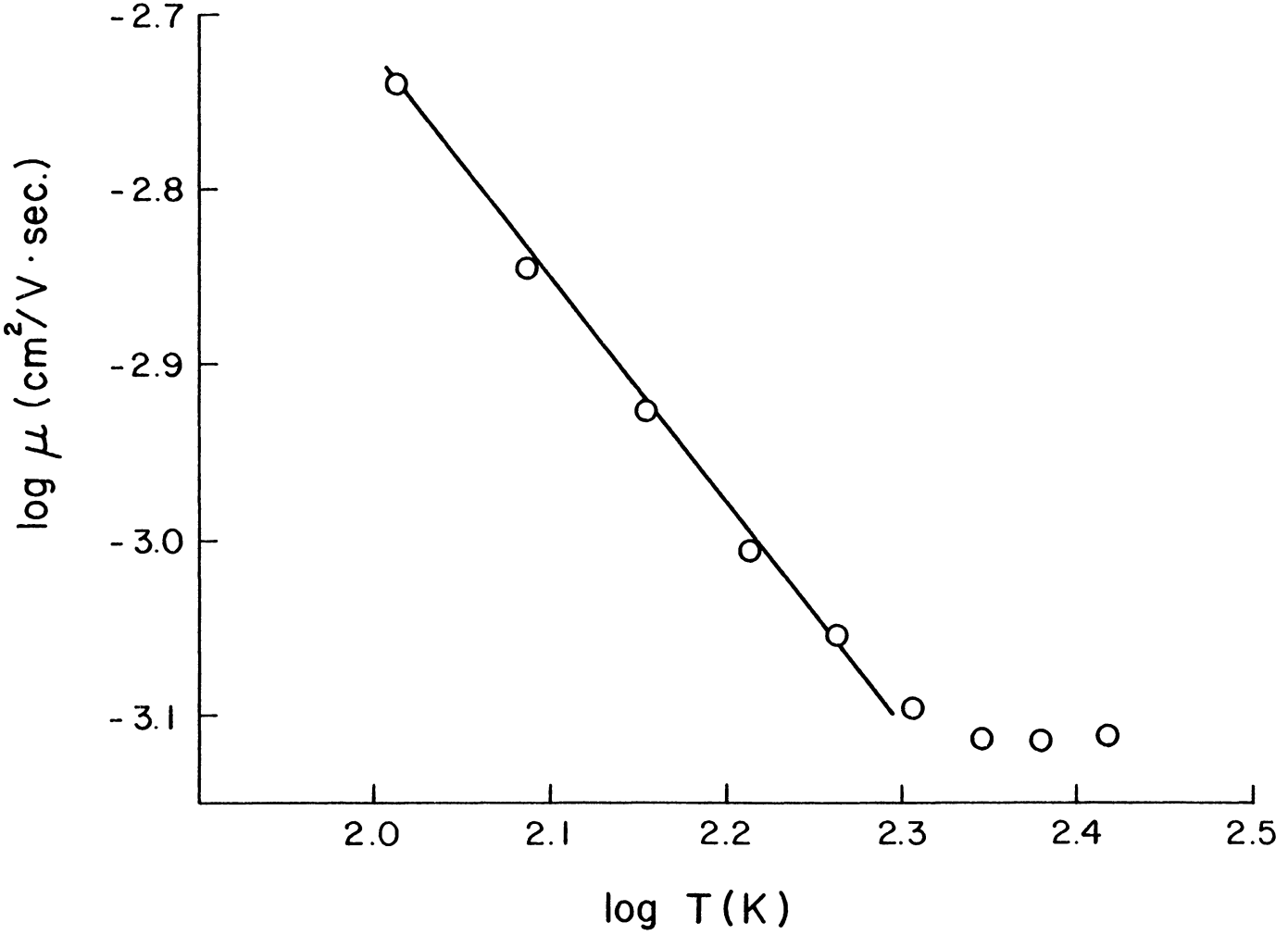


Figure 19. The logarithm of mobility versus the logarithm of temperature shows mobility to be proportional to $T^{-3/2}$ which indicates that lattice scattering is predominant. (3 μm film)

## 4.3 The Effect of Zn for $Zn_xCd_{1-x}S$ Films

Films of approximately equal thickness (between 14 μm and 17 μm) and of varying zinc content were measured. Room temperature values for the Seebeck coefficient, resistivity, carrier concentration, and mobility for samples 2-6, 3-1, and 3-2 can be found in Table III. Resistivity increases with zinc content as the mobility decreases. This is also the case found by Chynoweth and Bube in sprayed films.[11] The activation energy for the carrier concentration increases with zinc contents from .013 eV with x = 0 to .034 eV with x = .15. This is attributed to the increase in donor activation energy from 0.03 eV in CdS to 0.30 eV in samples with higher Zn proportions.[26] The barrier heights were found to be 0.029 eV, 0.049 eV, and 0.090 eV in the CdS, $Zn_{.04}Cd_{.96}S$, and $Zn_{.15}Cd_{.85}S$ samples respectively. This is in disagreement with Chynoweth and Bube's work on sprayed films.[11] They report that the barrier height is constant and the decrease in mobility is due to a decrease in the bulk mobility $\mu_o$. The bulk mobility for the samples reported in this paper decrease from 5.47 $cm^2$/volt·sec to 2.79 $cm^2$/volt·sec with increasing zinc content from x = 0 to x = .15. It is a combination of these two effects ($\phi_b$ and $\mu_o$) which account for the decrease in the measured mobility.

The increase in the grain boundary barrier height is partially due again (as in the CdS Films) to decrease in carrier concentration as the zinc content is increased. As the electron traps at the grain boundaries are filled the free electrons move more easily across the boundary.

TABLE III. Summary of $Zn_xCd_{1-x}S$ Film Results (Room Temperature)

| Sample | %Zn | Thickness (μm) | ρ(Ω-cm) | $\alpha(\frac{mV}{^oK})$ | $n(cm^{-3})$ | $\mu\ (\frac{cm^2}{volt \cdot sec})$ | $\mu_\Theta(\frac{cm^2}{volt \cdot sec})$ | $\phi_b$(eV) |
|---|---|---|---|---|---|---|---|---|
| 2-6 | 0 | 14.0 | 4.27 | -.255 | $1.05X10^{18}$ | 2.70 | 5.47 | .029 |
| 3-1 | 4 | 16.6 | 44.70 | -.330 | $3.58X10^{17}$ | 0.35 | 2.81 | .049 |
| 3-2 | 15 | 17.0 | $3.74X10^{2}$ | -.440 | $1.29X10^{17}$ | 0.11 | 2.79 | .090 |

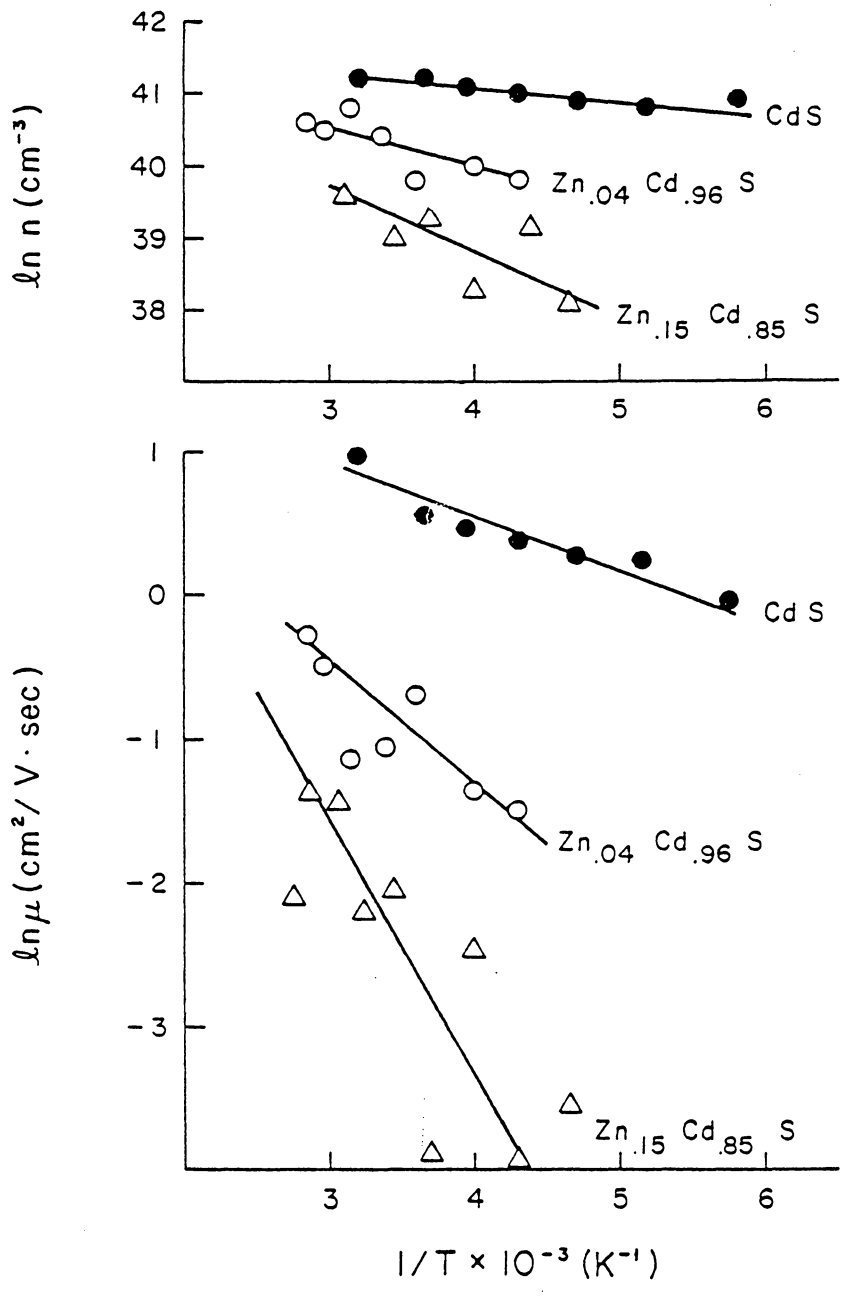


Figure 20. The logarithms of mobility and carrier concentration versus the inverse of temperature for the 14.0 μm CdS, 16.6 μm $Zn_{.04}Cd_{.96}S$, and 17.0 μm $Zn_{.15}Cd_{.85}S$ samples.

There may also be an increase in electron traps at the grain boundary due to the increase in zinc content.

# V. Conclusions

## 5.1 Results From This Work

The materials characteristics of mobility and carrier concentration are found in CdS and $Zn_xCd_{1-x}S$ films using the Seebeck effect. This effect is directly related to the carrier concentration (n) in the film and thus these measurements can be used with resistivity measurements to determine carrier mobility ($\mu$). An apparatus to measure the Seebeck effect and resistivity over a temperature range of 100 K to room temperature is designed and constructed. The Seebeck coefficient and resistivity are measured on an n-type single crystal silicon wafer. Results ($\alpha$ = -.707 mV/k at room temperature for a .005 $\Omega$-cm sample) compare favorably with samples measured by Brinson and Dunstan (-.650 mV/k at room temperature for a .005 $\Omega$-cm sample).[19] Six CdS samples and two $Zn_xCd_{1-x}S$ samples (x = .04 and x = .15) are measured. In all cases $\alpha$ increases with temperature. The resistivities of three CdS films are too high to make accurate Seebeck measurements. The carrier concentrations in the other three CdS films decrease with increasing film thickness. This could be due to 1) a larger defect or trap density in thinner films, 2) impurities from the substtrate which act as donors and would have a larger effect in thinner films, and 3) the greater possibility of a Cd rich film at the early stages of deposition. The carrier concentration decreases with Zn content. This is attributed to the increase in donor activation energy with increased Zn content.[26] The mobility increases with increasing film thickness in the CdS film samples. This is due mainly to increased grain size, and in part to

chemisorption of oxygen on the film surface causing a depletion layer. This has a greater effect in thinner films. Also surface scattering becomes more important in thinner films and this would cause a decrease in mobility. Mobility decreases with increasing Zn content which can be attributed to a decrease in bulk mobility from CdS to ZnS. Mobility is found to be grain boundary dependent ($\ell n\ \mu$ vs. 1/T is linear) in all films except in the thinnest CdS film. In this film mobility is found to be dependent on lattice scattering which follows a $T^{-3/2}$ dependence.

The grain boundary barrier height decreases in all cases with increased carrier concentration. As the film thickess is decreased in the CdS samples, the films have a higher number of free carriers and the barrier height decreases to a point where grain boundary scattering is no longer the dominate scattering mechanism. In the 3 μm sample lattice scattering becomes the dominate mechanism. As the concentration of zinc is increased in the $Zn_xCd_{1-x}S$ samples the carrier concentration decreases and the grain boundary barrier height is again increased. The added zinc may also increase the number of traps at the grain boundary.

From this work it can be concluded that:

1. An inexpensive design for the measurement of the Seebeck Effect and electrical resistivity in thin film samples is usable for making reliable mobility and carrier concentration calculations over a wide temperature range.
2. Carrier concentration decreases while mobility increases with increasing film thickness in evaporated CdS thin

films due to increased grain size and the diminishing effect of chemisorbed oxygen. As zinc is added to the film the carrier concentration and mobility decrease. This is due to an increase in donor activation energy as the zinc concentration is increased and to a decrease in mobility from a bulk sample of CdS to a bulk sample of ZnS.

3. The dominate scattering mechanism in all measured films, except the 3 μm film, is grain boundary scattering. In all cases the grain boundary barrier height decreases with increased carrier concentration. In the 3 μm film lattice scattering is the dominate mechanism.

## 5.2 Possible Future Work

The electrical characterization of the evaporated thin film CdS and $Zn_xCd_{1-x}S$ samples could be coupled with a more complete materials evaluation to more completely understand surface and grain boundary effects. ESCA and perhaps Auger profiles could reveal the exact nature of surface impurities causing a decrease in mobility in thinner films. Electron microprobe studies of the grain boundaries in the $Zn_xCd_{1-x}S$ films could reveal compositional changes which would aid in increasing the grain boundary barrier height as has been shown to occur as the zinc content in the film increases.

The measurement of the Seebeck effect on higher resistivity samples could be made possible by providing a mechanism to increase the imput impedance of the voltage measuring device. The complete shielding of all electrical connections and wires is of utmost importance and is a subject of continual concern.

The influence of illumination on the characteristics of mobility and carrier concentration is of interest because of the eutectual use of these films in photovoltaic solar cells. The effect of illumination is yet to be studied in $Zn_xCd_{1-x}S$ evaporater films and could yield very interesting results.

## References


1. D. R. Green, T. E. Michaels, L. C. Olsen, and L. S. Price, HEDL TC-1548, Final Report. DOE contract DE-AC14-76FF02170 (1980).

2. R. H. Bube, Electronic Properties of Crystalline Solids, Academic Press, Inc., New York (1974).

3. R. L. Petritz, Phys. Rev. 104, 1508 (1956).

4. J. W. Orton, B. J. Goldsmith, M. J. Powell, and J. A. Chapman, Appl. Phys. Lett. 37(6) (1980).

5. H. J. Goldsmid, Thermoelectric Refrigeration, Plenum Press, New York (1964).

6. R. R. Heikes and R. W. Ure, Jr., Thermoelectricity: Science and Engineering, Interscience, New York (1961).

7. L. H. Slack, Proceedings of the Third International College on Physics and Contemporary Needs, June 17 - July 6, 1978, Nathiagali, Pakistan, Plenum Press, New York (1979).

8. L. C. Burton, Solar Cells 1 (1979/80).

9. H. B. Kwok and R. H. Bube, J. Appl. Phys., Vol. 44, No. 1 (1973).

10. Chen-ho Wu and Richard H. Bube, J. Appl. Phys., Vol. 45, No. 2 (1974).

11. T. A. Chynoweth and R. H. Bube, J. Appl. Phys., Vol. 51, No. 3 (1980).

12. R. H. Bube, Electronic Properties of Crystalline Solids, Academic Press, Inc., New York (1974) pp. 220-244.

13. T. C. Harman and J. M. Honig, Thermoelectric and Thermomagnetic Effects and Applications, McGraw-Hill, New York (1967) Chap. 1-3.

14. L. J. van der Pauw, Philips Res. Rep. 13, 1 (1958).

15. Patrick M. Hemenger, Rev. Sci. Instrum., Vol. 44, No. 6 (1973).

16. S. S. Devlin, Physics and Chemistry of II-VI Compounds, Wiley, New York (1967) p. 561.

17. C. A. Wert and R. M. Thomson, Physics of Solids, McGraw-Hill, New York (1970) p. 268-270.

18. Blakemore, Semiconductor Statistics, Pergamon Press, New York (1962).

19. M. E. Brinson and W. Dunstan, J. Phys. C: Solid St. Phys., Vol. 3 (1970).

20. D. J. Howarth and E. H. Sandheimer, Proc. R. Soc. A 219, 53(1953).

21. W. P. Bleha, W. H. Hartman, R. L. Jamenez, and R. N. Peacock, J. Vac. Sci. and Tech., Vol. 7, No. 1 (1970).

22. J. P. Legré and S. Martinuzzi, Phys. Stat. Sol. (a) 1, 689 (1970).

23. D. M. Hughes and G. Carter, Phys. Stat. Sol. 25, 449 (1968).

24. G. H. Blount, R. H. Bube, and A. L. Robinson, J. Appl. Phys. 41, 2190 (1970).

25. J. Martinez and J. Piqueras, Solid-State Elect., Vol. 23, 297 (1980).

26. E. A. Davis and E. I. Lind, J. Phys. Chem. Solids 29, 79 (1968).

The vita has been removed from the scanned document

# THE SEEBECK EFFECT IN THIN FILM CdS AND $Zn_xCd_{1-x}S$

by

Scott Preston Moore

(ABSTRACT)

Seebeck and resistivity measurements are made on thin film CdS and $Zn_xCd_{1-x}S$ samples in an apparatus of original design over a temperature range from near liquid nitrogen temperature to room temperature. The temperature dependence of mobility and carrier concentration is studied in CdS films of varying thicknesses (3 μm to 14.0 μm) and in $Zn_xCd_{1-x}S$ films of varying zinc content ($0 \leq x \leq .35$). Scattering is found to be grain boundary dependent in all films except the thinest CdS film measured (3.0 μm) in which lattice scattering dominates. The grain boundary barrier height increases with film thickness in CdS films due to a decrease in carrier concentration as film thickness increases making electron traps at the grain boundary influential. As the zinc concentration is increased the carrier concentration decreases and the grain boundary barrier height increases as seen in the CdS films.